FABRICATION OF ELECTROSPUN POLY(GLYCEROL SEBACATE) (PGS) SCAFFOLDS FOR CORNEAL TISSUE ENGINEERING

by

SUMEYYE NARIN

Submitted to the Graduate School of

Engineering and Natural Sciences in partial

fulfilment of

the requirements for the degree of Master of Science

Sabanci

University

July 2024

FABRICATION OF ELECTROSPUN POLY(GLYCEROL SEBACATE) (PGS) SCAFFOLDS FOR CORNEAL TISSUE ENGINEERING

Approved by:

Asst. Prof. S i b e l C E T I N E L . . . .

(Thesis Supervisor)

Prof. Gozde INCE . . . .

Assoc. Prof. Sakip ONDER . . . .

Date of Approval: July 18, 2024

ABSTRACT

FABRICATION OF ELECTROSPUN POLY (GLYCEROL SEBACATE) (PGS) SCAFFOLDS FOR CORNEAL TISSUE ENGINEERING

SUMEYYE NARIN

MATERIALS SCIENCE AND NANO ENGINEERING M.Sc.
THESIS, JULY 2024

Thesis Supervisor: Asst. Prof. SIBEL CETINEL

Keywords: electrospinning, artificial tissue, membrane, fiber, elastomer

The demand for tissue engineering of cornea grows daily. Various applications have been implemented to meet this need with biomaterials such as polymers. Amongst those polymers, poly (glycerol sebacate) (PGS) has been used to perform various tissue engineering applications owing to their biodegradable, biocompatible, elastomeric, transparent, and pro-regenerative properties. Electrospinning of PGS would enhance the mechanical strength, permeability, and cell attachment to the scaffold. Electrospinning PGS alone remains challenging due to its very low molecular weight (MW) and low glass transition temperature (T_g). Thus, carrier polymers like poly (vinyl alcohol) (PVA) have been widely used in PGS electrospinning research. For these reasons, in this work, blending of PGS and PVA as a supporter polymer in electrospinning was investigated to mimic corneal membranes. The best blending ratio with the optimized electrospinning parameters was determined to be 55% PGS and 45% PVA. Because of the thermal crosslinking property of the PGS, a crosslinking temperature of 160°C led to the best performance in terms of fiber stability, porosity and membrane transparency amongst temperatures of 140, 150, 160 and 170°C in the membranes. After crosslinking, PVA ought to be removed to increase transparency of the

membranes. Therefore, several washing methods were applied and the most PVA removal was obtained through 48 h water wash at room temperature (RT). The membranes obtained by this process had resulted in 28% porosity with average fiber diameter of 4 µm; and the mechanical strength of the membranes was found to be 1.2 MPa with a 20% strain at most. Moreover, the measured permeability of the membranes on average was 1.03E-06 cm^2/s which is highly close to the actual permeability of cornea as 3.02E-06 cm^2/s. Results of biocompatibility tests were performed with human corneal epithelial cells (HCEpCs) indicated that cells were almost 50% viable after 2 weeks of incubation time and collagen coating process. As a result of optimized electrospinning of PGS:PVA blend, we obtained a microporous, tough and biocompatible membrane.

ÖZET

KORNEA DOKU MÜHENDİSLİĞİ İÇİN PGS MEMBRANLARININ ELEKTROSPİN İLE ÜRETİMİ

SÜMEYYE NARİN

MALZEME BİLİMİ VE NANO MÜHENDİSLİK YÜKSEK LİSANS
TEZİ, TEMMUZ 2024

Tez Danışmanı: Asst. Prof. SİBEL ÇETİNEL

Anahtar Kelimeler: elektrospinning, yapay doku, membran, fiber,

elastomer

Kornea için doku mühendisliği ihtiyacı gün geçtikçe daha da artmaktadır. Polimerler gibi biyomalzemelerle çeşitli uygulamalar bu ihtiyacı karşılamak için yapılagelmiştir. Bu polimerlerin içinden poli (gliserol sebasat) (PGS) membranlar, biyolojik olarak parçalanabilen, biyouyumlu, elastomerik, şeffaf ve pro-rejeneratif özellikleri nedeniyle çeşitli doku mühendisliği uygulamalarını gerçekleştirmek için kullanılmıştır. PGS'i tek başına electrospin etmek PGS'in çok düşük moleküler ağırlığa (MW) ve düşük cam geçiş sıcaklığına (Tg) sahip olması nedeniyle hayli zordur. Bu sebeple, poli (vinil alkol) (PVA) gibi taşıyıcı polimerler PGS'in electrospin edilmesi araştırmalarında yaygın olarak kullanılmıştır. Bu nedenlerden dolayı, bu çalışmada kornea zarlarını taklit etmek için PGS'in destekleyici bir polimer olarak PVA ile karıştırılarak electrospin özellikleri araştırılmıştır. Optimize edilmiş elektrospin parametreleri ile en iyi karışım oranı önceden yapılan çalışmalarla %55 PGS ve %45 PVA olarak belirlenmiştir. PGS'nin termal kürlenme özelliği nedeniyle, 160°C'nin kürleme sıcaklığı, 140, 150, 160 ve 170°C sıcaklıkları arasında fiber dayanıklılığı, gözeneklilik ve membran şeffaflığı açısından en iyi performansa yol açtığı gözlemlenmiştir. Thermal kürlemeden sonra, membranların şeffaflığını artırmak

için PVA çıkarılması gerekmektedir. Bu nedenle, birkaç yıkama yöntemi denendi ve içlerinden en çok PVA giderimi oda sıcaklığında (RT) 48 saat su yıkama yoluyla elde edildi. Bu işlemle elde edilen membranlar ortalama fiber çapı 4 olan %28 porozite ile sonuçlanmış; membranların mekanik mukavemeti ise 1.2 MPa ve elastisitesi %20 bulunmuştur ki bu değerler bu güne kadar literatürde belirtilen değerler içinde en yükseğidir. Dahası, membranların geçirgenliği ölçüldüğünde ortalama olarak 1.02E-06 cm^2/s ölçülüp korneanın gerçek geçirgenliği olan 3.02E-06 cm^2/s değerine oldukça yakın olduğu gözlemlendi. İnsan kornea epitel hücreleri (HKEpH) ile biyouyumluluk testlerinin sonuçlarında ise, hücrelerin 2 haftalık inkübasyon süresinden sonra neredeyse %50 canlı olduğu gözlemlenmiştir. Özetlendiğinde PGS:PVA karışımının optimize edilmiş elektrospininin bir sonucu olarak, HCEpC'ler için yüksek bir canlılık oranına sahip mikro gözenekli, sert ve biyouyumlu bir membran elde edildi.

ACKNOWLEDGEMENTS

I would like to thank those who supported me during my MSc. thesis period. First of all, I would like to emphasize my sincere appreciation to my supervisor Asst. Prof. Sibel Çetinel for her guidance, sincerity, and motivation. She supported me to overcome all difficulties I faced in my research. I am thankful to my teammates Kamal Asedi-pakdel, Ebru Demir Dede, and Sevilay Burcu Şahin for their help in the understanding of the project and contributions to my research.

I also would like to express my gratitude to my parents Dudu and Hasan Hüseyin Narin, my siblings Refika and Musab Akbaba, Muhammet and Rumeysa Narin, my dearly nieces and nephew, Ayşe Ravza, Asım, Zeynep and Zehra for their emotional support and always waiting for my return. My final thanks go to those who made my life at Sabanci the best years of my life – my dear friends. My dear roommate Gülnur Şener for being always patient with me and being the biggest support, and my friends Aybüke B. Özer, Gülşah Yıldız, Cemile Uslu, Elif B. Kıvrak, and A. Baki Şahin, thank you all for the fun we had together and for making me a better person.

To my future self…

TABLE OF CONTENTS

LIST OF TABLES

1. LIST OF FIGURES

2. LIST OF ABBREVIATONS

°C Degrees Centigrade

ALK Anterior Lamellar Keratoplasty

ASTM American Society for Testing and Materials

BET Brunauer-Emmett-Teller Analysis

BM Bowman's Membrane

CCK-8 Cell Counting Kit-8

DM Descemet's Membrane

DMEK Descemet's Membrane Endothelial Kerotaplsty

DSAEK Descemet's Stripping Automated Endothelial Keratoplasty

ECM Extracellular matrix

FBS Fetal Bovine Serum

FECD Fuchs Endothelial Corneal Dystrophy

FT-IR Fourier Transform Infrared Spectroscopy

h Hours

HCEnCs Human Corneal Endothelial Cells

HCEpCs Human Corneal Epithelial Cells

HFIP Hexafluoroisopropanol

ICC Immunocytochemistry

kPa Kilo Pascal

kV Kilovolt

min Minutes

mL, mg Milli-liters, -grams

MPa Mega Pascal

MW Molecular Weight

N Newton

nm, μm, mm, cm Nano-, Micro-, Milli-, Centimeter

PCL Polycaprolactone

PEG Poly (ethylene glycol)

PGS Poly (glycerol sebacate)

PK Penetrating Keratoplasty

PLGA Poly (lactic-co-glycolic acid)

PLLA Poly (L-lactic acid)

PMMA Poly (methyl-methacrylate)

PNIPAAm Poly(N-isopropylacrylamide)

polyHIPE poly high internal phase emulsion

PVA Poly (vinyl alcohol)

RT Room Temperature

SEM Scanning Electron Microscopy

TE Tissue Engineering

Tg Glass Transition Temperature

UTS Ultimate Tensile Strength

wt% weight percent

1. INTRODUCTION

1.1. Cornea

The human cornea is a transparent and avascular tissue protecting the eye from mechanical damage and infections [1]. Corneal epithelium, stroma and corneal endothelium, respectively from outside to inside, are the three layers of cornea and connected by acellular structures: Bowman's and Descemet's membranes (Fig. 1.1) [2]. The epithelium is a squamous, and stratified tissue that covers 10% of overall cornea. It is accountable for water regulations, transfer of soluble compounds, and serves as physiological barrier [3]. The condition of being outermost layer involves relation with external surroundings, therefore, it is more vulnerable to trauma such as corneal ulcer, dystrophies, abrasion, and erosion. Such injuries mostly result in severe implications such as vision blurriness or vision loss [4, 5]. Posterior to epithelial basement membrane, there exists an acellular Bowman's layer (also called anterior elastic lamina by W. Bowman [6]) which is composed of amorphous collagen fibrils and is 15 µm in thickness. It rests as a support for epithelium and stroma fibrils for anchoring [7].
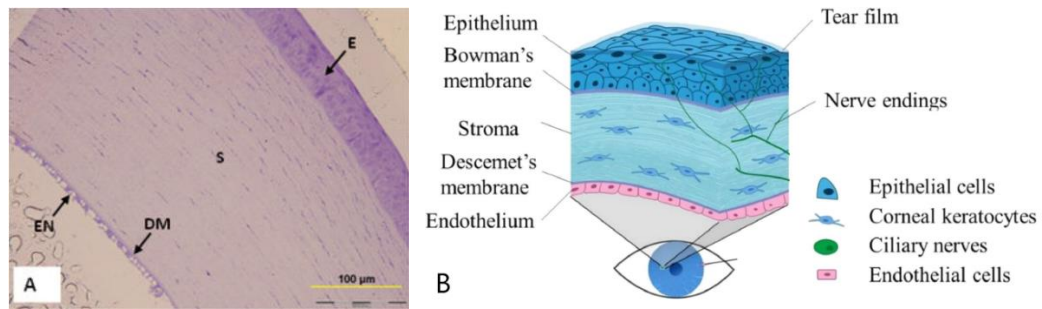
Figure 1. 1. Corneal layers. Light micrograph of tree shrew cornea **(A)** which consists of epithelium, Bowman's layer, stroma, Descemet's membrane, and endothelium. E=Epithelium, S=Stroma, DM=Descemet's membrane, and EN=endothelium. Reproduced from Almubrad et al. [2] under CC BY-NC-ND. © Molecular Vision.
Representative figure of corneal layers **(B)**, which was reproduced with permission from Zhang, B. et al. [8] © Elsevier.

The intermediate region of cornea consists of the least number of cells called keratocytes is stroma and it substantially constitutes 95% of the cornea [2]. This layer is mainly composed of uniformly distributed collagen fibrils which are regulated by proteoglycans. Its high-oriented structure reduces forward light scattering and enhances the mechanical strength and transparency [9]. It comprises of 80 % water and has excellent swelling properties with a viscoelastic behavior. Its stiffness increases when people age, causing cornea to be deprived of its elasticity and transparency [10]. At the posterior of the stroma, Descemet's membrane is found which is rich in type VIII collagen and it provides a basement for endothelium attachment [11].

The innermost layer, endothelium, operates as hydration level controller by removing water from stroma for correct level of transparency [3, 12]. Diseases like fuchs endothelial corneal dystrophy (FECD), glaucoma, and diabetes mellitus are corneal endothelium linked disorders damaging the endothelium. Injuries like these lead to permeability increase and immense cell pump activity causing a swollen and thick stroma which could bring about vision loss [13, 14].
The reported numbers for surgical operations that have been performed to treat corneal diseases are over 180,000 globally [15]. Numerous methods have been developed to replace the injured corneal tissue with a donor such as Descemet's membrane endothelial kerotaplsty (DMEK), Descemet's stripping automated

endothelial keratoplasty (DSAEK), and anterior lamellar keratoplasty (ALK) [16]. These techniques are derived from the penetrating keratoplasty (PK) which is full thickness corneal replacement and still used in cases where stroma is scarred. If only endothelial layer is defected, then lamellar techniques such as DSAEK and DMEK are preferred. For all techniques, the process includes either transfer just the Descemet's layer or Descemet's membrane and some part of stroma with usually less than 100 µm [17-19]. These techniques have mostly been used in the replacement for allotransplants, however, new practices with synthetic material-based transplants have also been reported [20, 21] for several reasons. First of all, allogenic transplants which are human-based donors are highly likely to experience corneal graft rejection and failure which is frequently caused by the loss of epithelial cells from the donor layer [22, 23]. Another reason is that the number of donor corneas is insufficient caused by the high demand for corneal transplants which leads to long waiting lists for a suitable donor [24]. Therefore, interest in tissue engineering applications has increased in regenerative medicine to improve the quality of the patient's life. Numerous tissue engineering (TE) applications with synthetic or natural material-based scaffolds, decellularized scaffolds and cell-based scaffolds have been provided. These engineered scaffolds support the injured site mechanically and enhance cell proliferation which will increase the long-term success of transplants [25, 26].

1.2. Corneal Tissue Engineering

Natural polymer-based studies mostly dominate corneal TE research due to their biodegradability allowing the healing of injured site slowly by itself [27]. One of the first studies in this aspect is a PEG stabilized collagen-chitosan hydrogel which was studied by Rafat et al. They observed this implantable hydrogel both in vivo and in vitro experiments as an elastic, tough and transparent graft [28]. In another study with collagen, researchers acquired a decellularized scaffold and implanted it surgically. On the other hand, three

months after surgery, they observed the degradation of the graft due to host rejection [20]. One of the significant achievements in corneal TE for long-term monitoring is reported by Fagerholm et al. with 1-year [29, 30] and 4-years (Fig. 1.2) [21] of follow up studies proving the safety of the alternative compared to donor organ transplantation. These studies prove the potential of collagen type-I as a corneal tissue construct material yet, it requires complicated chemical crosslinking steps and has limited use due to high cost [31].
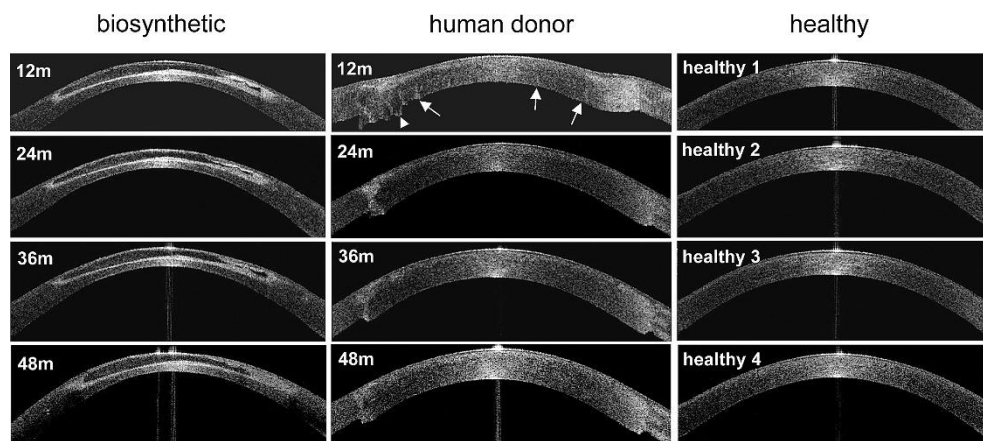
Figure 1. 2. Comparison of 4 years of implanted, donor and healthy cornea anterior segment optical coherence tomography images. Reproduced with permission from Fagerholm, P. et al.[21] © Elsevier.

Research on corneal TE with synthetic polymer-based scaffolds also has been conducted, yet only in vitro studies have been performed. These polymers included poly(methyl-methacrylate) (PMMA), poly(lactic-co-glycolic acid) (PLGA), and polycaprolactone (PCL). The PMMA resulted in being the most toxic polymer with an experiment on human corneal endothelial cells (HCEnCs). The PLGA scaffolds, in the same experiment, were composed of the thinnest fibers and enabled HCEnCs proliferation the most, however, the price of the material draws a disadvantage on feasibility [32]. Another successful candidate for corneal TE to date is poly(N-isopropylacrylamide) (PNIPAAm)

with clinical applications with corneal epithelial cells yet complex crosslinking process challenges the applicability of the polymer [33]. Therefore, a biomaterial to fulfill the requirements for corneal TE is still being searched.

1.3. Poly(glycerol sebacate) PGS as Corneal TE

In recent years, an elastomer named poly(glycerol sebacate) (PGS) has been synthesized by Wang et al.. PGS as an elastomeric biopolymer is also biodegradabile and biocompatibile (Fig. 1.3) [34]. The elasticity and strength of the polymer has revealed its potential use in soft tissue applications [35]. The transparency of this material increases its potential usability as retinal [36] or corneal [37] tissues. This polymer possesses the properties of thermoset elastomers [38], and it is relatively affordable due to the natural sources of its monomers [34]. Moreover, studies both in vitro and in vivo indicated that the PGS degrades into its monomers which are glycerol and sebacic acid, which exist inherently in the human body [34, 35, 39].
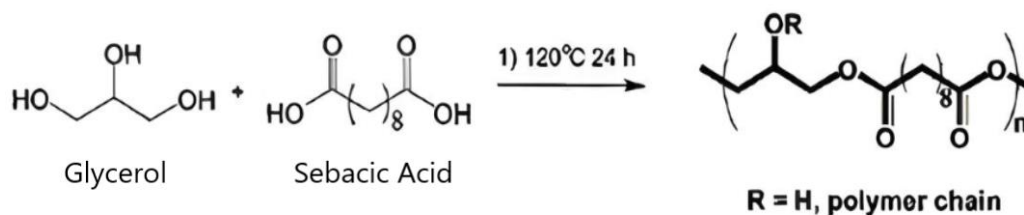
Figure 1. 3. Chemical reaction structure of the prePGS synthesis. The end groups of glycerol and sebacic acid react at 120°C for 24 h and produces poly (glycerol sebacate). Reproduced with permission from Wang, Y. et al. [34] © 2023 Springer Nature.

The polymer is synthesized by the esterification of glycerol and sebacic acid through a reversible reaction of the primary hydroxyl groups in glycerol with carboxyl groups in sebacic acid, resulting in polyester and water as a by-product [34]. It requires a second crosslinking step due to low glass transition

temperature (Tg) making it a viscous fluid which cannot retain its shape. Generally, it is crosslinked at temperatures around 120-130 ℃ for 24-48h [34, 40]. Hydrolytic degradation rate of cross-linked polymer is slower than pre-polymer, indicating the increased stability and strength of the polymer [41]. In addition, this polymer can be tailored to acquire higher mechanical properties following various degradation rates for different applications.

The crosslinked nature of the PGS defines its mechanical properties and degradation time. It is directly dependent on crosslinking temperature and duration [42, 43]. Various studies have been conducted to observe the effect of temperature and time on crosslinking density at a range of 110-150°C and 20 min-144h [34, 44-48]. The study of Chen et al. indicated that Young's modulus of the polymer increased from 0.056 MPa to 1.2 MPa. They achieved this by the increase in crosslinking temperature from 110°C to 130°C, yet the elasticity of the polymers decreased accordingly (Fig. 1.4) [48]. Other studies which crosslinked PGS at 120°C for 42-48h obtained similar ultimate tensile strength (UTS) around 0.45 MPa and strain of 200% [34, 45, 47, 48].Meanwhile the increase of temperature to 150°C dropped elasticity significantly to 50% [44]. Another study on crosslinking duration effect on mechanical properties of PGS indicated an increase in the tensile strength by 0.4 MPa and a decrease in elasticity by 40% when the duration increased from 42h to 144h [45]. All these research has proven the impact of temperature and duration on crosslinking density which is the deviation on rigidness and degradation rate of the material.
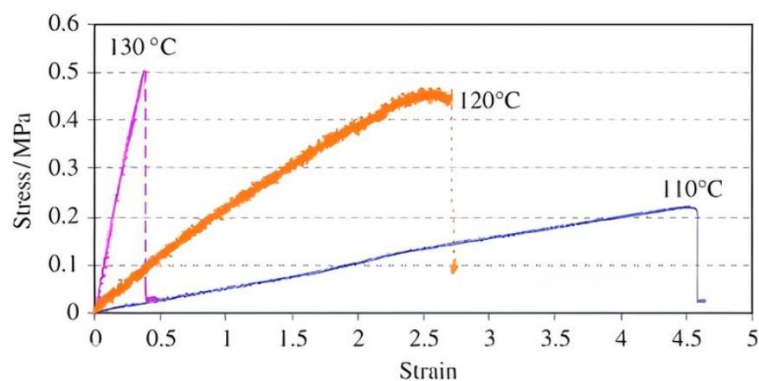
Figure 1. 4. Comparison of crosslinking temperature impact on PGS toughness. Reproduced with permission from Chen, Q. et al.[48]

In the literature, the reported numbers for the molecular weight of the PGS with the conventional synthesis method are not high due to the polycondensation polymerization. The conventional synthesis method as reported in 2002 by Wang Y. et al. has mostly resulted in low molecular weight around 1K to 18K g/mol [34, 49-51]. While the 1:1 glycerol sebacic acid molar ratio is used as a conventional synthesis method, different molar ratios (2:1, 2:2, 2:3, 2:4, and 2:5) were performed at 120°C in three steps to understand the synthesis of PGS. These five prepolymers including different molar ratios were low molecular weight oligomers, containing two to nine repeating units [40, 49].

However, with the addition of a catalyst to the system like a lipase enzyme as in the study of Ning Z. et al., achieved a high molecular weight (59K g/mol) within 67h of reaction. They maintained the reaction in equimolar reaction conditions at 150 °C for the first 1 h and the resulting monophasic bulk reaction mixture was incubated at 120°C for 24h (prepolymerization). Then, the reaction temperature was reduced to 90°C, before adding the catalyst N435 (Candida antarctica lipase B) to retain its activity. And then, starting from the 100 Torr, the pressure applied throughout the reaction by reducing its time to time [52]. Perin G. et al. and Lang K. et al. resulted in higher molecular weights with the use of same enzyme such as 56K to 92K g/mol within 55 to 96h of synthesis by reducing the pressure in every 12h till 25 Torr obtained and different molar ratios of sebacic acid, glycerol and catalyst (0.5: 0.5: 1.0, 0.33: 0.66: 1.0, 0.25: 0.75: 1.0, and 0.2: 0.8: 1.0) [53, 54]. Although the MW of pPGS was increased by these methods, the reaction time also increased significantly. A longer reaction time undermines the practicality of the synthesis process, especially in time-sensitive applications.

Until this day, the PGS has been used as a scaffold for a wide variety of tissues such as cardiac [48, 55], vascular [56], cartilage [38], adipose [57], retinal [36, 58], and cornea [37, 59-61]. One of the studies on PGS has proven the viability of the polymer with human corneal epithelial cells with a rate of 90% [37, 60]. A significant parameter for corneal tissue is the permeability of the layers for the

regulation of water uptake. Therefore, it requires the scaffold to be porous rather than smooth films. To accomplish this property, polymers have been fabricated with a variety of methods including hydrogels [62], bioprinting [63-65], lithography [66], and electrospinning [67-69].

1.4. Electrospinning of PGS

To resemble the structure of extracellular matrix (ECM) and increase permeability, scaffolds can be constructed by electrospinning. It is an electrostatic fabrication technique that can create ultra-fine fibers from various materials like polymers. It is a simple process where a polymer solution or melt is ejected through a nozzle under a high-voltage electric field, which stretches the material to into thin fibers that are collected on a grounded target. It is commonly employed in creating nanofibers for applications in areas such as tissue engineering, filtration, and drug delivery due to tunable properties. Other techniques such as salt-leaching or polyHIPE creates pores which can enhance permeability, however, considered as mechanical defects in terms of strength [70, 71]. Therefore, electrospinning the PGS will allow the corneal membranes to be tough and an appropriate environment for cell attachment and proliferation.

Numerous factors influence the process of electrospinning including solution (viscosity, conductivity, molecular weight, and surface tension), process (applied electric field, flow rate, and tip to collector distance), and ambient parameters (humidity and temperature) (Fig. 1.5). Manipulation of these parameters enables the production of fibers with targeted features and applications. Increasing the concentration, and MW of the polymer causes viscosity to rise as well resulting in larger and more uniform fiber diameter [72]. Very low viscosity prevents electrospinning by producing no fibers, and very high viscosity creates difficulties in the ejection of polymer solution from the ejectors [73, 74]. The increase in the applied voltage causes greater stretching and leading to narrower fiber diameters and vice versa [75]. Types of collectors also

plays a role in the fiber diameter and alignment increasing the stretching by a rotating mandrel type [76].
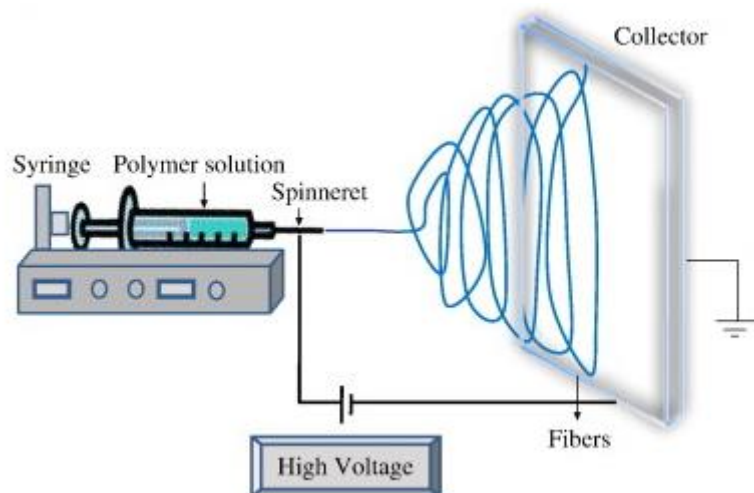
Figure 1. 5. Representative image of an electrospinning setup. Reproduced with permission from Bhardwaj, N. et al.[77]

The low molecular weight of uncured PGS lead to solutions with low viscosity disabling it to electrospin [78]. Once cured, PGS forms an elastomer preventing it to be dissolved in organic solvents [79]. Another point to be considered in terms of electrospinning PGS as stated before is that PGS has a low Tg making it flow below room temperature and disabling crosslinking of fibrous structure due to fibers merging into each other [34]. Hence, PGS cannot be electospun by itself and requires other polymers to support the PGS in mechanical strength.

1.4.1. Blending PGS with Carrier Polymers for Electrospinning

Therefore, several approaches including a high molecular weight polymer as a carrier have been proceeded to solve this problem including polycaprolactone (PCL) [31, 80] , poly(L-lactic acid) (PLLA) [57, 81] and poly(vinyl alcohol) (PVA)

[67, 68]. Salehi et al. characterized PGS-PCL blend scaffolds for corneal stroma structure and optimized a fibrous scaffold. They researched electrospinning of PGS-PCL by different weight ratios (1:1, 2:1, 3:1, and 4:1) to enhance the elastic properties of nano-sized fibers for corneal TE. They indicated both cell lines, human corneal epithelial cells (HCEpCs) and HCEnCs, have been affected positively and even the HCEpCs established monolayers within 3 days [59]. The addition of chitosan to the PGS-PCL blend in another study provided that although PGS-PCL blending indicates good results for HCEpC culturing, further research is needed on the blend of PCL with chitosan [61]. Another polymer blended with PGS for electrospinning is PLA in the research of Denis et al. Different blending ratios of PLA-PGS allowed to observe the collapsing fibers due to increase in the PGS and to find the ideal ratio to be 50:50 [81]. Frydrych et al. searched the compatibility of PGS with PLLA for adipose TE which resulted in microporous structures rather than fibers [57].

1.4.2. PVA-PGS Blending for Tissue Engineering Applications

Another potentially proven polymer is PVA by being biocompatible, biodegradable and nontoxic which is approved by the US Food and Drug Administration [82]. The PVA has higher crosslinking temperature than PGS and it can be dissolved in water simplifying its removal from the system. These are the reasons carrying PVA one step ahead of other polymers in terms of electrospinning with PGS. Yadong Wang, who contributed to the synthesis of PGS for the first time, and his colleagues constructed a highly elastic membrane by electrospinning PGS with PVA (Fig. 1.6) [67]. They attempted to remove the PVA for membrane properties to be similar to that of PGS, however, could not succeeded the 100% removal. Another study which investigated fiber stability and diameter after PVA removal resulted in a reduction as one-quarter of the original fiber diameters [68]. Both studies proved the viability of this combination by fibroblast cell viability assessment. PVA-PGS blend was also studied for neural TE which provided slow and continuous degradation rate pacing with tissue regeneration time [83, 84].

28
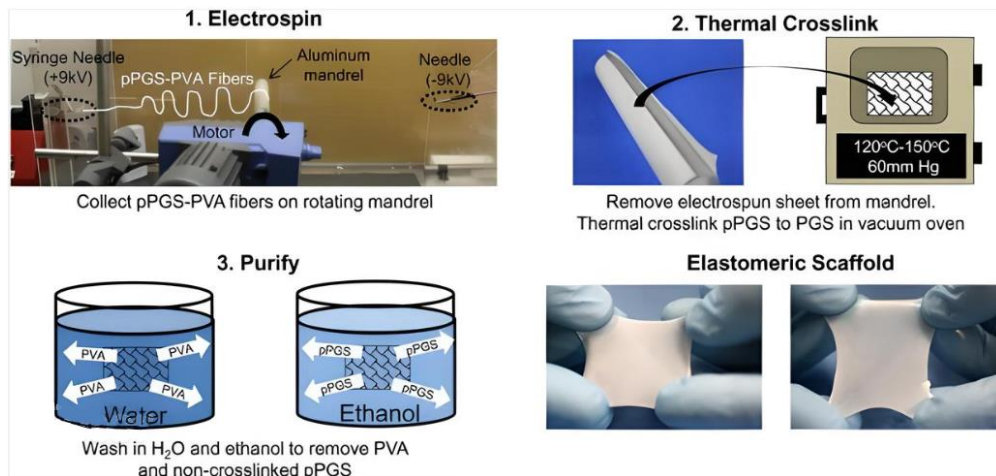
Figure 1. 6. Fabrication of fibrous PGS-PVA sheets for vascular tissue engineering studies. Reprinted with permission from Jeffries, E. M. et al.[67]

1.5. Aim of the Thesis

Until now, electrospun PGS membranes have been studied with different carrier polymers for corneal tissue engineering, yet their blend with PVA has not been studied for corneal scaffolds. In this study as in figure 3.1, we combined PGS with PVA for mechanical support to secure the fibrous network during crosslinking with a ratio of 55:45. Thereby, we aimed to obtain a similar scaffold as in the Bowman and Descemet's membranes by electrospinning by investigating the effect of temperature on fiber retention after crosslinking and PVA removal from the membranes.

2. MATERIALS AND METHOD

2.1. Materials

PVA (Mw = 90 000, degree of hydrolysis = 98%), glycerol (purity 99%), sebacic acid (purity 99%), toluene (purity 99%), and hexafluoro isopropanol (HFIP) were purchased from Merck (Germany). The sulfuric acid (H_2SO_4, purity 95-98%) was purchased from Isolab Laborgeräte GmbH (Germany).

2.2. Membrane Fabrication

2.2.1 Synthesis of pre-PGS (pPGS)

For electrospinning, 1:0.8 glycerol: sebacic acid was dissolved in toluene (16X of glycerol amount) in a beaker which was covered with aluminum foil and stirred at 180°C. After the monomers dissolved in the toluene, $H2SO4$ (with the 1.1 x 10-3 ratio of glycerol) was added into solution. After 10 min mixing, small holes were made on the aluminum cover of the beaker. The reaction continued for 35 min at 180°C temperature under open air. The molecular weight of the resulting pre-polymer was characterized to be ~50,000 g/mol by GPC (Appendix A).

2.2.2 Fabrication of PGS Membrane

The fibrous membranes were obtained by electrospinning pPGS-PVA blend, thermally crosslinking the membrane and PVA removal. A 5.8 wt% 55:45

pPGS to PVA blend was prepared by dissolving the polymers in 8, 16, and 24ml of HFIP overnight. Electrospinning was proceeded with following parameters: 3.5 mL/h flow rate, 24 kV voltage, 20 cm distance and 18G needle. The electrospun fibers were collected on an aluminum foil coated rotating mandrel with a diameter of 10 cm at 500 rpm speed. The concentrations and parameters were decided by preliminary studies which is not shown in this study.

The fibrous membranes were removed from the mandrel and placed in a pre-heated, vacuum oven at 140-160°C and 5 mb for 48 hours for crosslinking. PVA was removed from the membranes with water wash for 24-48 h by gentle mixing. For heated washings, the water was heated up to 60°C while washing the membranes.

2.3. Membrane Characterization

2.3.1. Crosslinking and PVA Removal

The chemical bonds and groups of PGS and PVA were confirmed using a *Fourier Transform-InfraRed* (FT-IR, Thermo Scientific / iS10, USA) spectroscopy with a frequency range of 400–4000 cm−1 at 4 cm−1 resolution. The pPGS and PGS polymers were also characterized to determine the crosslinking degree.

2.3.2. Morphology and Fiber Size Measurements

The fiber morphology and size of the membranes were evaluated by scanning electron microscopy (SEM, Zeiss / Leo Supra VP35, Germany). Samples were placed onto conductive carbon tape on the aluminum stabs. Then, they are coated with Au/Pd sputter coater (Cressington 108 Sputter Coater, UK) in 3.5 nm thickness (40 mA for 120 s). Fiber diameters were determined by Image J software (NIH, Bethesda, MD) as an average of 20 measurements for each group.

2.3.3. Porosity Measurements

The porosity of the membranes was analyzed via SEM image analysis in the ImageJ software (NIH, Bethesda, MD). The porosity is further determined by Brunauer-Emmett-Teller (BET, Micromeritics 3Flex, USA) analysis.

The samples were dried in the oven overnight under vacuum. The samples, then, placed in the BET tubes (Micromeritics 3Flex 3500 Sample tube, Flat Bottom, 12 mm, USA) and degassed overnight at 100°C. After degassing, the tubes are placed in the BET machine within liquid nitrogen. Analysis was conducted with BJH Isotherm analysis parameters of nitrogen gas as adsorptive in 77,203 K.

2.3.4. Permeability Measurements

The procedure was followed as shown in Fig. 2.1. Firstly, the 48 h washed samples were dried and washed with ethanol for an hour for sterilization and then dried in the air. The samples, then, placed in between the Valia-Chien permeability chambers (PermeGear Inc., 2 mL volume, USA) and covered with parafilm to prevent any leakage. One of the chambers was filled with only FBS where the other one was filled with 10 mg/mL glucose in FBS. The glucose amount in the only FBS was measured throughout the experiment. The first measurement was taken immediately after FBS poured in the chamber by a glucose meter (Accu-Chek, Roche, Switzerland). Then, measurements were taken in periods of 30 min x3, 60 min x3 until the glucose amount reaches 400-500 mg/dL.
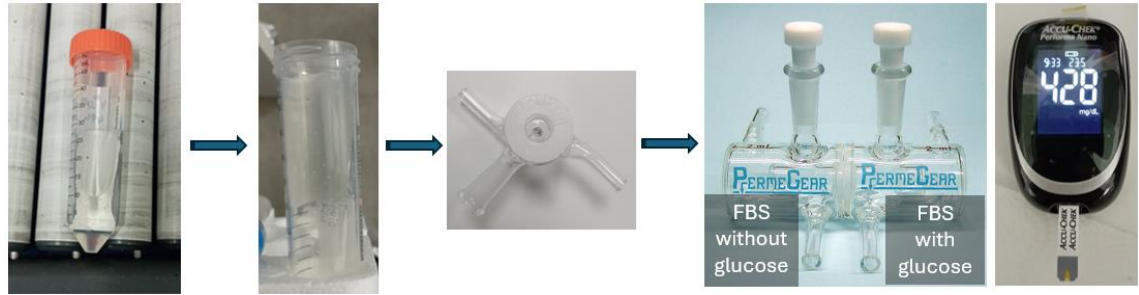
Figure 2. 1. Visual presentation of permeability assay. The samples were washed with 70% ethanol for 30 min and then air dried for about an hour until it is totally dry. After placing the membrane in between chambers, one side is filled with FBS and other side is filled with FBS+glucose, and measurements taken from the side with FBS with glucose by a glucose meter.

The diffusion coefficient was calculated by the following formula which was used to calculate cornea permeability where D is for diffusion coefficient, L is the sample thickness, C is the initial concentration , Q is the amount of glucose passing through the membrane per time (slope of the graph), and A is the area of diffusion [85].

$$D = \frac{Q \; x \; L}{C}, where \; Q = \frac{dC/t}{A} \qquad (Eq.1)$$

2.3.5. Mechanical Properties

Mechanical stability of the membranes was characterized by uniaxial tensile test via Mark 10, Series 7 (USA) digital force gauge. A rectangular sample of 30 mm length and 125 mm width was prepared according to the ASTM D882 standards for films with a thickness less than 1 mm. 50 N load was applied with a rate of 10 mm/min. Each test was evaluated in triple (n=3). The stress of the membranes was calculated as load/(membrane length x thickness) in N/mm^2 as shown in Fig. 2.2.
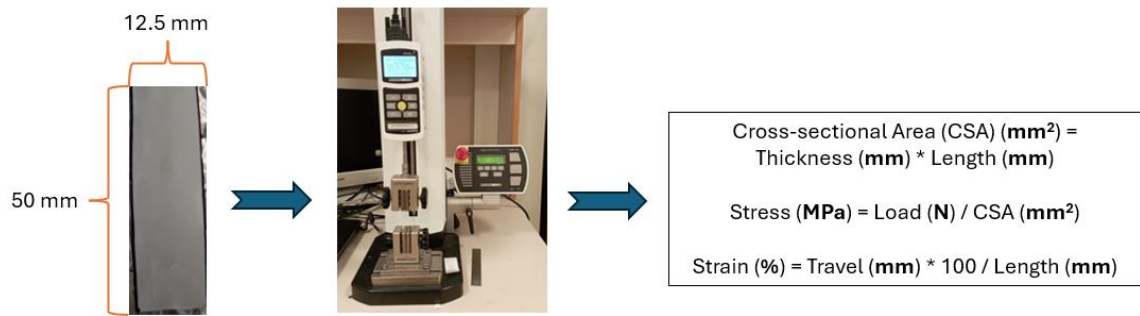
Figure 2. 2. Visual presentation of tensile test with Mark-10 instrument. The membranes were cut in ASTM standards for thin membranes and then pulled in a tension test for mechanical measurements. The calculations used to convert the measurement data are also given.

2.3.6. Biocompatibility Measurements

Biocompatibility tests for the PGS membranes were performed with human corneal epithelial cells. PGS membranes were sterilized in 70% ethanol for an hour and exposed to UV radiation for 30 minutes on each side. Then, membranes were incubated in cell culture media at 37°C.

To evaluate the cell attachment to the membranes, HCEpCs were acquired from Afsun Şahin Lab at Koç University Hospital, Istanbul, Turkiye. The cells were incubated in DMEM-F12 growth media containing 10 ng/ mL EGF, 10% FBS and 1% penicillin-streptomycin antibiotic solution. The HCEpCs were incubated on PGS membranes which placed on a hydrophobic plate to increase cell attachment to membranes. This incubation proceeded with different durations for different groups such as 2h, and overnight. And then, cells on the membranes were placed in a hydrophilic 48-well plate for 2-weeks of incubation in total. A cell counting assay was performed by CCK-8 kit (Abcam, ab2228554). At the end of 1-week and 2-weeks of incubation, the growth media on the wells were removed and membranes were washed with PBS once to discard cell debris. The viability reagent in the kit was diluted with growth media in the ratio of 1:10. Then, it is inserted into the samples with an incubation of 4h. At the end of incubation, these solutions were placed in a 96-well plate for absorbance measurement at 450 nm in a spectrophotometer

(Tecan, Infinite 200 Pro). The statistical analysis was performed with a negative control group of membranes without cells and positive control group of cells without membranes. The incubation of the PGS samples were proceeded with the help of Sevilay Burcu Şahin.
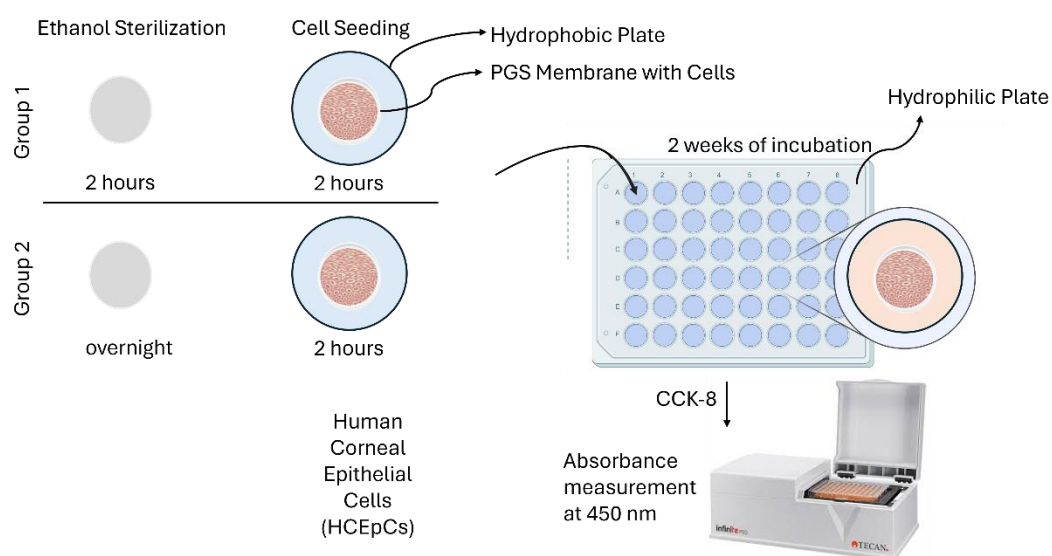
Figure 2. 3. Preparation of PGS membranes for cell viability assays

The PGS membranes incubated for 14 days with epithelial cells were visualized under SEM to observe cell attachments. The cells were fixed with series of ethanol (50, 60, 70, 80, 90, 95, 100% EtOH: water) following 2.5% glutaraldehyde in EtOH (Sigma-Aldrich, Merck, Germany) and then, hexamethyldisilazane (HMDS, Sigma-Aldrich, Germany) (50, 60, 70, 80, 90% for 10 min, 100% for overnight). The fixed samples were examined by SEM.

3. RESULTS

3.1. Membrane Fabrication

3.1.1. Synthesis of pre-PGS and Fabrication of PGS Membrane

To prepare the membranes, the pPGS was synthesized and blended with the PVA in the ratio of 55:45. The various electrospinning parameters including concentration, flow rate, applied voltage, and distance have been found to be playing a significant role on the spinning, fiber stability and diameter [77]. Therefore, these parameters were optimized specifically for this mixture and found to be 5.8 wt% concentration, 3.5 mL/h flow rate, 24 kV voltage in 20 cm distance. The mixture was electro-spinnable; however, the solution was thickened in the nozzle within a minute which prevented further spinning so it required cleaning frequently. The fibers were collected on the mandrel type collector to increase alignment of fibers and to decrease the fiber diameter. The collected fiber sheet was placed in the pre-heated oven to crosslink the fibers. The reason to pre-heat the oven was to prevent PGS fibers melting down at around 60°C before they crosslinked at 140-160°C so that fibers would be exposed to 140-160°C directly.
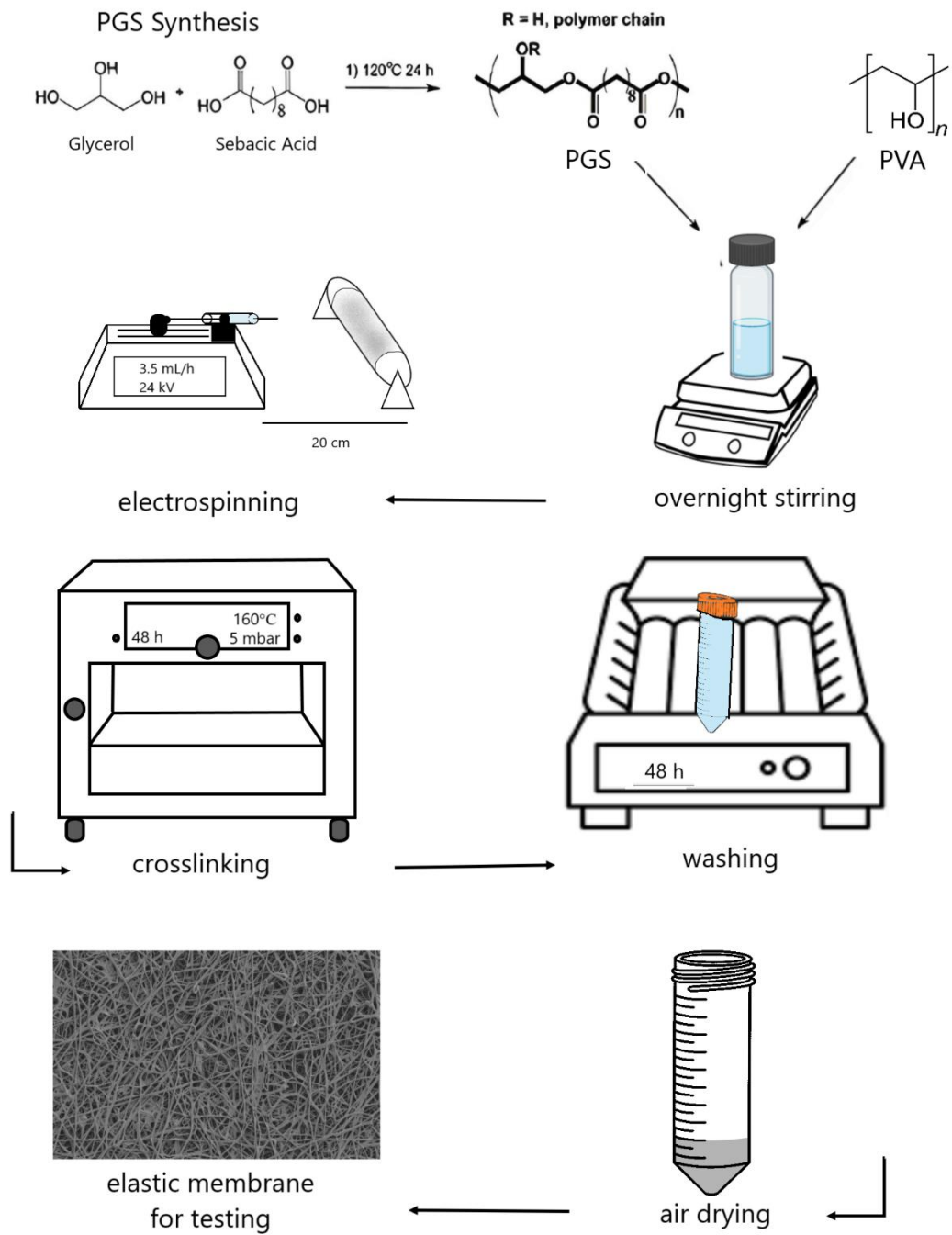
Figure 3. 1. Graphical abstract for the fabrication of fibrous PGS-PVA sheets as corneal membranes.

3.2. Membrane Characterization

3.2.1. Crosslinking and PVA Removal

The resulting PGS-PVA fibrous sheets were characterized by FT-IR spectroscopy. The PGS and PVA have generally similar peaks which caused peak differentiation to be harder as can be seen in Figure 3.2.1. The peak observed in between 3500 cm^{-1} and 3000 cm^{-1} due to -OH stretching exists in both polymers [67]. However, the OH stretching peak is mainly focused at 3450 cm^{-1} for PGS and at 3300 cm^{-1} as a broader peak for PVA. The crosslinked membrane by blending PGS and PVA had a peak closer to the PVA by residing around 3350 cm^{-1} and being broader. Another similarity can be observed at around 2900 cm^{-1} and 2800 cm^{-1} corresponding to alkane stretching. This peak is mainly focused at 2900 cm^{-1} with a small peak on the left where it is clearly two-shouldered for PGS. The crosslinked membrane also resembles the PGS in shape, however, shifted to left due to PVA focusing on 2900 cm^{-1}. The only characteristic peaks for PGS resided at 1740 cm^{-1} and 1200 cm^{-1} for -C=O, and -C-O stretching due to carboxylic acid group of sebacic acid in PGS [67, 83]. The peaks at the range of 1100 cm^{-1} and 900 cm^{-1} in the characteristic region corresponds to -C-O stretching as well due to primary and secondary -OH groups in both PGS and PVA [57, 67, 68]. The characteristic small peak at 840 cm^{-1} is specific to PVA and observed in the crosslinked membranes as well [68].
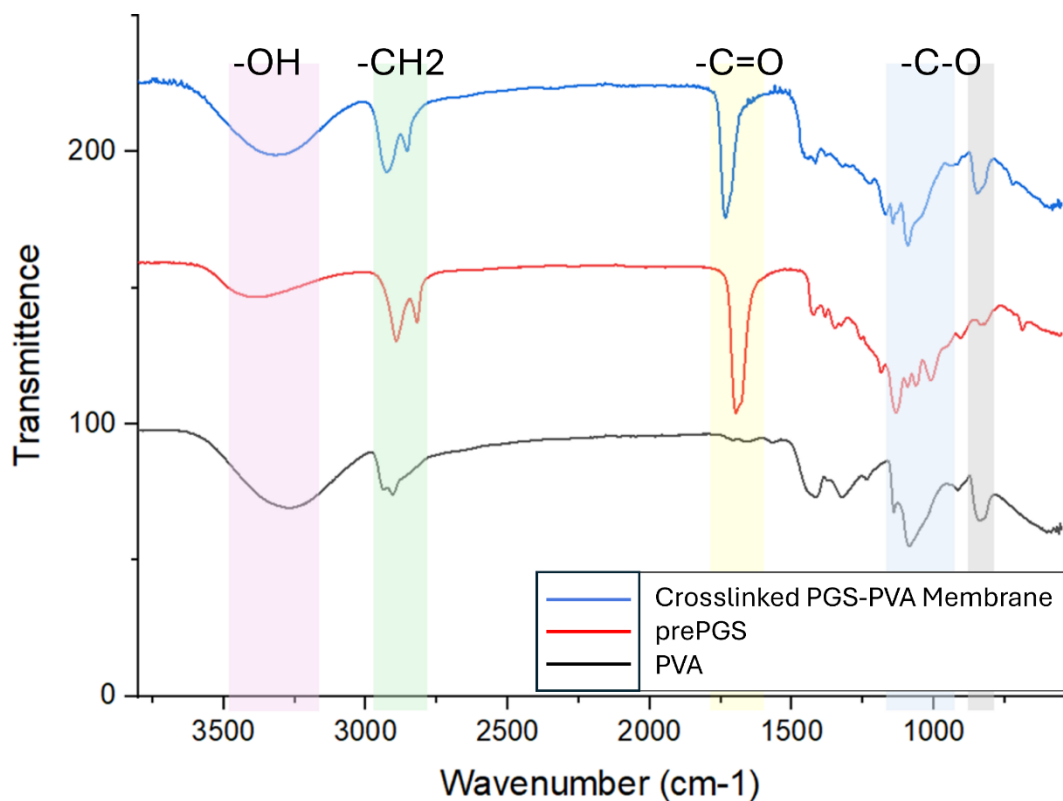
Figure 3.2.1. FT-IR spectra of crosslinked membranes in comparison with pure PGS and PVA (with stacked lines by Y axis offsets)

After obtaining stable fibrous sheets with 8 mL spinning, we decided to obtain tougher PGS fibers for better membrane stability. For this purpose, we investigated the crosslinking temperature effect first considering two factors: crosslinking density and fiber stability (after crosslinked and PVA removal). It has been proven with research that thermoset polymers such as PGS indicate different properties according to crosslinking density. As the temperature increased, crosslinking of PGS was also increased as stated in the literature [44]. The PGS exhibits a broad peak around 3500 cm^{-1} and a sharp peak at 940 cm^{-1} in FT-IR spectroscopy due to the presence of secondary -OH groups' stretching which is origin of crosslinking [86]. Therefore, when the crosslinking degree is increased, a reduction in the OH peak is expected. In figure 3.2.2, the OH peak reduction can be observed as the temperature increases from 140°C to 160°C indicating 160°C provided the highest crosslinking. However, when the temperature of crosslinking set to 170°C, there is no reduction in the peak which might be due to start of PVA crosslinking.
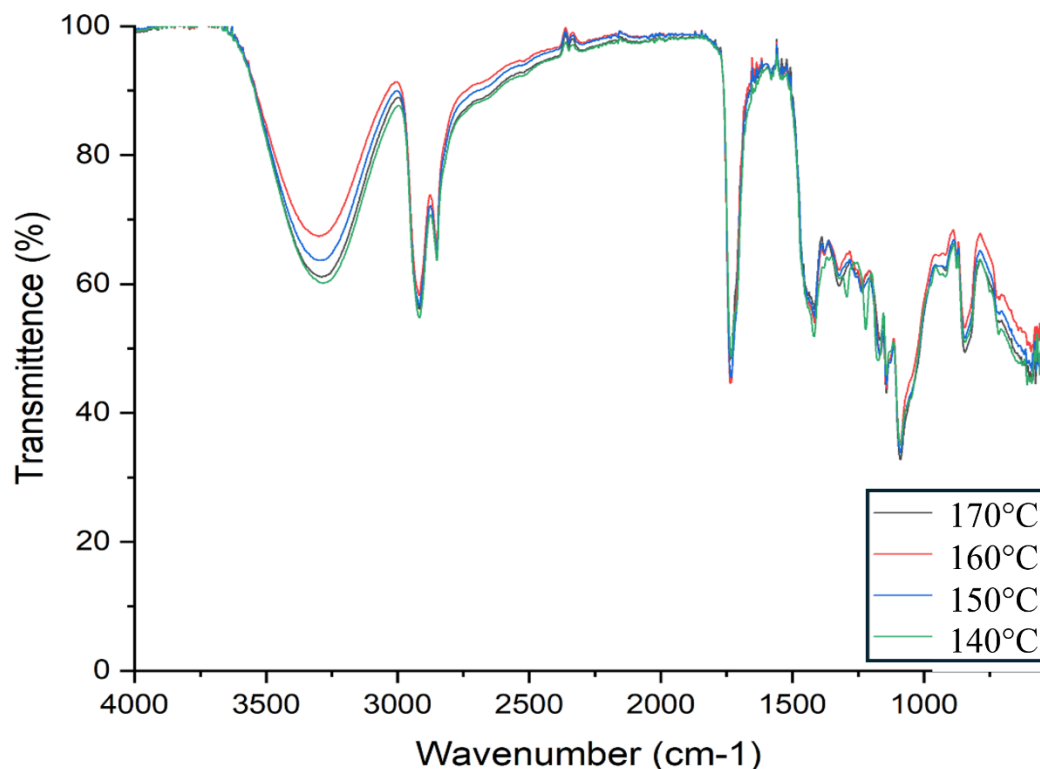
Figure 3.2.2. The FT-IR spectrum of membranes crosslinked at 140-170°C. Crosslinking temperature optimization with 8 mL after 48 hours of water washing at room temperature.

The PVA removal is important to obtain pure PGS and thereby increase elasticity, and transparency of the membranes. These properties play a significant role in the mimicking of cornea. It is reported that PVA-PGS membranes did not cover all properties of the pure PGS and need to be removed from the system following series of washings [34, 67]. As PVA can be dissolved simply in water without requirements of organic solvents which might be toxic, 3 different washing methods applied. The PVA removal was examined in FT-IR spectroscopy as well. Washing the membranes in water for 24 h caused a reduction at the peaks 3300 cm^{-1} (Fig. 3.2.3.b) due to -OH stretching of PVA and at the peak 840 cm^{-1} (Fig. 3.2.3.d) indicating -C-O stretching of PVA [68]. The peak further decreased when the membranes washed for 48 h in water. The 24 h and 48 h of water washings were supported with ethanol wash to remove residual PGS monomers which resulted in a

diminishment at the peak 1730 cm^{-1} (Fig. 3.2.3.c) corresponding to -C=O stretching due to sebacic acid presence.
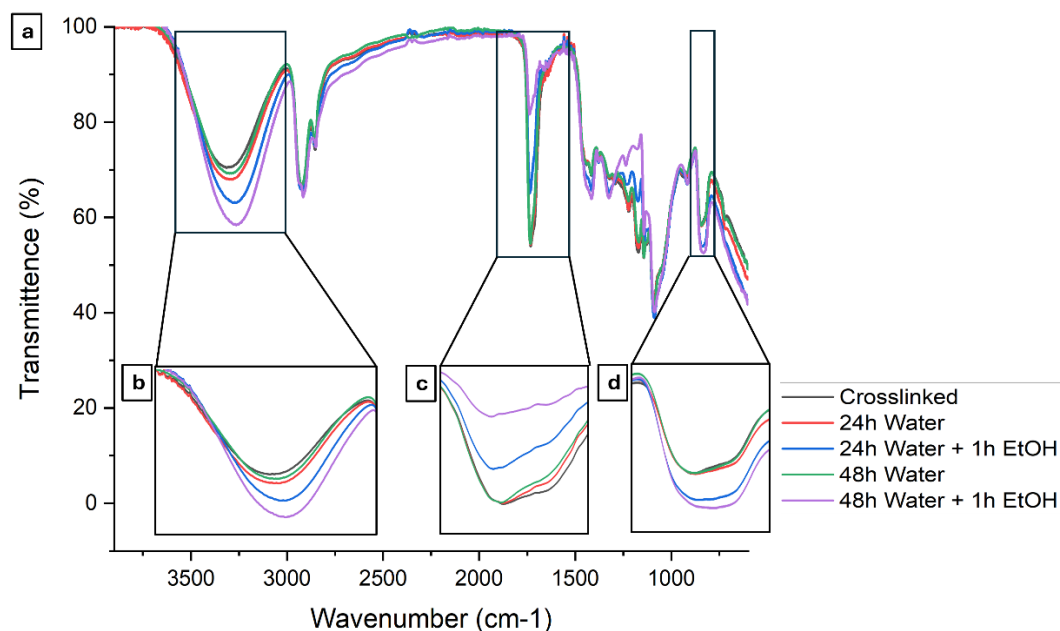
Figure 3.2.3. Washing Optimization with 24 mL (a) Overall spectra of PVA, PGS, and membranes with different washing applications, **(b)** comparison of the peak intensity at 3300 cm^{-1}, **(c)** at 1730 cm^{-1}, and **(d)** at 840 cm^{-1}

The samples were also characterized to observe the fiber stability and morphology after exposing a set of temperatures (Fig. 3.2.4). The crosslinking temperatures of 140°C, 150°C and 160°C displayed good fiber stability, and scaffold mechanical integrity after crosslinking instead of being fused into a sheet as in 170°C. Due to changes in the fiber structure and morphology post-washings, the membranes were also examined.

The crosslinking at 140°C was not enough to support the fibrous structure. After the washing steps fibers collapsed and a less porous membrane was obtained. Although the membrane crosslinked at 150°C could resist more than the membrane crosslinked at 140°C for long hours of washing, it shared a similar destiny in heated and room temperature washings for 24h. The membrane crosslinked at 170°C was able to retain its morphology after

41

washing steps; however, the morphology after crosslinking was not sufficient to provide a membrane for good porosity. The best temperature which could withstand heated and long hours of washings to remove the PVA was observed at 160°C.
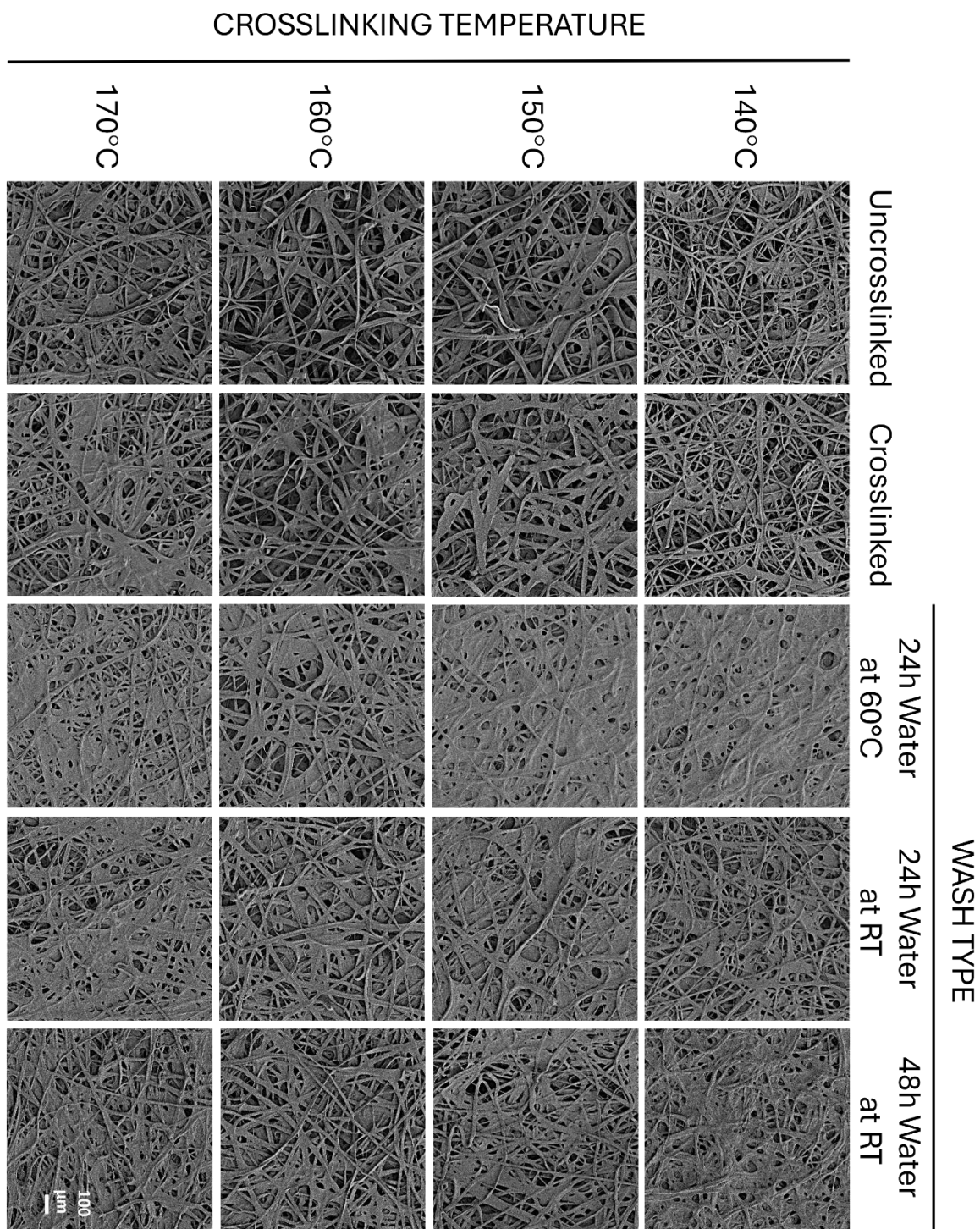
Figure 3.2.4. SEM images of crosslinking temperature (140, 150, 160 and 170°C) and washing optimization (24h heated, 24h room temperature and 48h room temperature) with 8 mL

43

We increased the spinning solution amount to 16 mL and 24 mL to increase the thickness of the membrane to achieve high strength and elasticity. The normal cornea thickness would reach to only 0.536 mm on average [87, 88], Bowman layer to 15 µm thickness, and Descemet's membrane to 10 µm thickness [3]. It is significant to achieve toughness in the membrane to obtain appropriate barrier function of cornea, defending the eye from mechanical damages and infections [1]. The membranes that we obtained with 8 mL of spin solution were extremely sensitive to force even held in the hand. Hence, it was a must to increase the thickness of the membrane to increase mechanical strength despite the fact that the natural corneal layers are thinner. The membrane which was spun with 8 mL of spin solution had 30 µm. This value increased to 60 µm with 16 mL, and to 82 µm with 24 mL spins (Fig. 3.2.5).
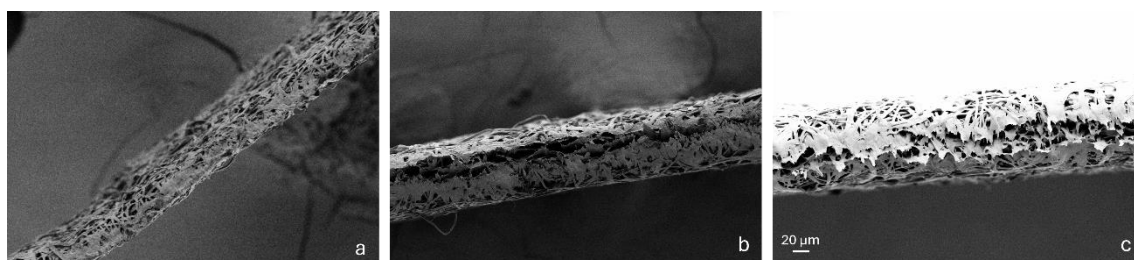
Figure 3.2.5. The cross-sectional SEM images of different amounts of (a) 8 mL-29 µm, (b) 16 mL-59 µm, and (c) 24 mL-82 µm spin solutions with different measurements from various parts of membranes, repeat of spins and average of 4 measurements each.

As the amount augmented, the PGS would not be able to crosslink sufficiently to preserve its shape since it would be harder for heat to reach inner sections of membrane. This could have required extra time for crosslinking, yet the fiber morphology was not highly affected by the change in the spinning solution amount (Fig. 3.2.6). The repeatability of the 82 µm spinning was also followed with SEM which resulted in similar morphology and fiber diameters (Appendix B).
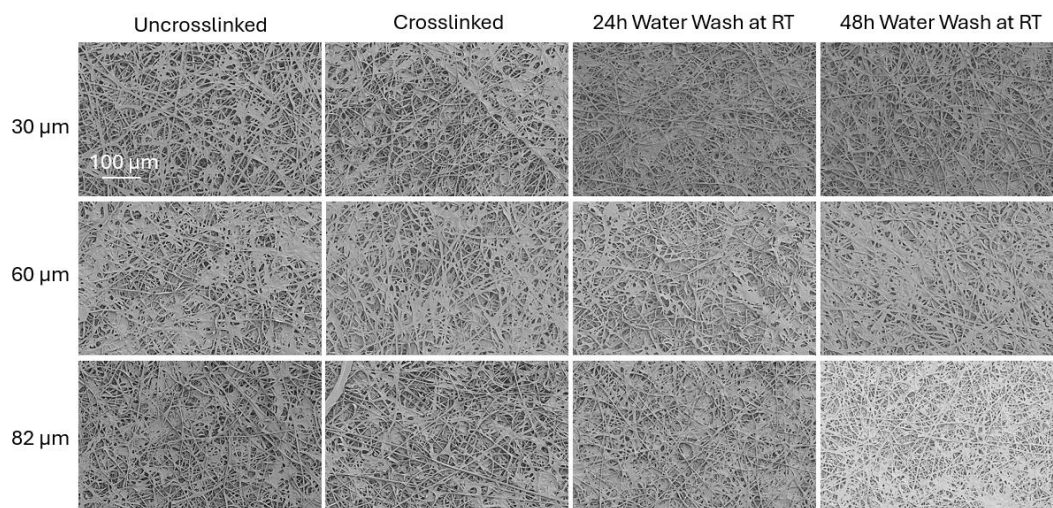
Figure 3.2.6. SEM images of washes with comparison of membrane thickness.
(We removed 24 h heated wash because it was requiring an extra treatment though giving the same results with 24 h room temperature wash)

3.2.2. Transparency Measurements

The effect of different crosslinking temperatures was examined by transparency measurements as well. When the fibers fuse into the sheets, membranes become more transparent due to reduced reflection of light in a less porous environment. Therefore, 140°C and 170°C crosslinking temperatures generated more transparent membranes (Fig. 3.2.7.a). The SEM data of these two temperatures confirmed the presence of fused fibers. Accordingly, 150°C and 160°C led to less transparent membranes when compared to 140°C and 170°C temperatures; however, still transparent enough to read the writings under the membrane.

The transparency of the membranes after thickness increase was also inspected. Due to the increase in the porosity of the membrane, the transparency is expected to decrease accordingly. As assumed, the transparency of the membranes decreased with increased thickness (Fig. 3.2.7.b).
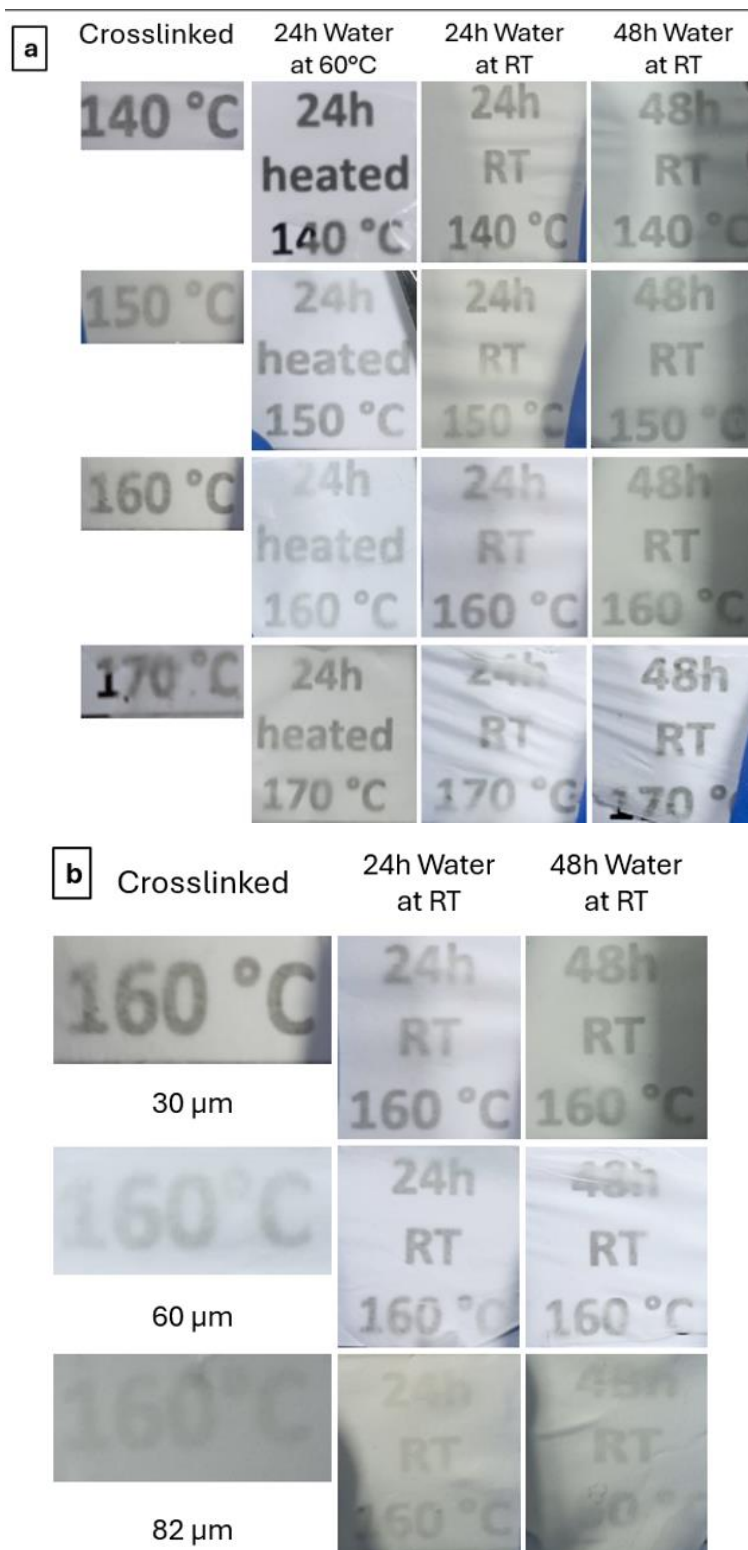
Figure 3.2.7. Transparency of membranes with different crosslinking temperature and washings (a) with 30 µm, (b) only 160°C temperature crosslinking and washings with 30-, 60-, and 82- µm thick membranes.

As a result of crosslinking temperature and thickness evaluations, a 160°C crosslinking temperature and a 24 mL spinning volume was determined to result in best crosslinking density and fiber stability. Therefore, further characterizations on the membrane were proceeded with the membranes prepared with 24 mL spin solution, 160°C crosslinking temperature and 48h room temperature washing.

3.2.3. Porosity and Fiber Size Measurements

The morphology of the membranes has significance in terms of corneal usage of membranes as it influences the cell attachment, and proliferation. Thus, porosity and fiber diameters of the membranes were evaluated. The porosity of the membranes were characterized by both BET analysis and from the SEM images by ImageJ software to be precise instead of calculating by a method using bulk density as in the study of Salehi et al. [89].

In Table 1, the percent porosity of the 30 µm thick membranes resulted in 28.4% porosity where it is slightly dropped to 24.4% in 60 µm thick membrane, however, it recovered to 29.5% in 82 µm thick membrane. The porosity on average was 27.4 by ImageJ measurements. The results of BET analysis supported these data by giving close results as 29.2, 28.7 and 28.7% for 30-, 60-, and 82-µm thick membranes, respectively. The average porosity of membrane by BET analysis was also close to the SEM image analysis with a slight increase to 28.8%. Even though the thickness was increased, the percent porosity did not change significantly proving the success of repeatability of the spinning in different conditions.

Table 1. Percent porosity of the membranes measured by ImageJ software from SEM images as analytical measurement and BET instrument as experimental measurement with 30-, 60-, and 82-µm thick membranes

	30 µm	60 µm	82 µm
SEM (%)	28.4 ± 1.5	24.4 ± 2.3	29.5 ± 2.06
BET (%)	29.2	28.7	28.7

The fiber diameter of membranes were measured by the ImageJ as well. Electrospinning of pPGS blended with PVA at the ratio of 55:45 facilitated fibers at 3.9 ± 3 µm thickness (Fig. 3.2.8). The fiber diameter did not exhibit significant variation among groups (30-, 60-, and 82 µm thickness membranes). The 60-, and 82 µm – thick membranes sustained the initial diameter range as in 30 µm thick membranes (4.02 µm) with a greater distribution within the range (4.27 µm for 16 mL and 4.35 µm for 24 mL) which also proves the repeatability of the spinning.
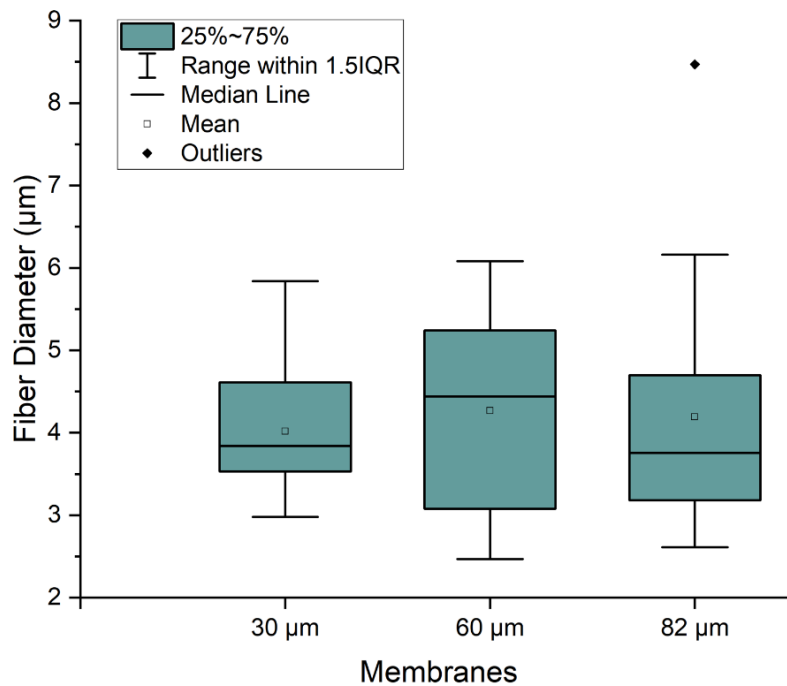
Figure 3.2.8. Distribution of fiber diameter measurements of each spins. 20 measurements for 30-, 60-, and 82 µm thick membranes were taken and represented with box-chart (with a range of (+1.82)-(-1.03 µm) for 30 µm, ±1.80 µm for 60- and 82 µm)

3.2.4. Permeability Measurements

The continuous nutrient supply provides the corneal epithelial cell integrity. Glucose is the primary molecule for energy in the epithelium and it arrive to the epithelium by diffusing through the stroma and endothelium [85]. Therefore, it is vital to assess the rate of glucose diffusion through these membranes. The graph in figure 3.2.9. presents the diffusion rate of glucose through 82 µm thick membranes (a) and 60 µm thick membrane (b). The slope of the graph provides information about the glucose diffusion rate of the membrane. This value is used to calculate the diffusion coefficient by Eq.1. The resulting coefficient value for 60 µm thick membrane was 1.19E-06, and for 82 µm thick membrane repeats 9.80E-07, 1.15E-06, and 8.14E-07, respectively. The average of these values, which is 1.03E-06 is highly close to the real cornea diffusion coefficient value of 3.02E-06, therefore, indicating the success of electrospun membranes in terms of permeability.
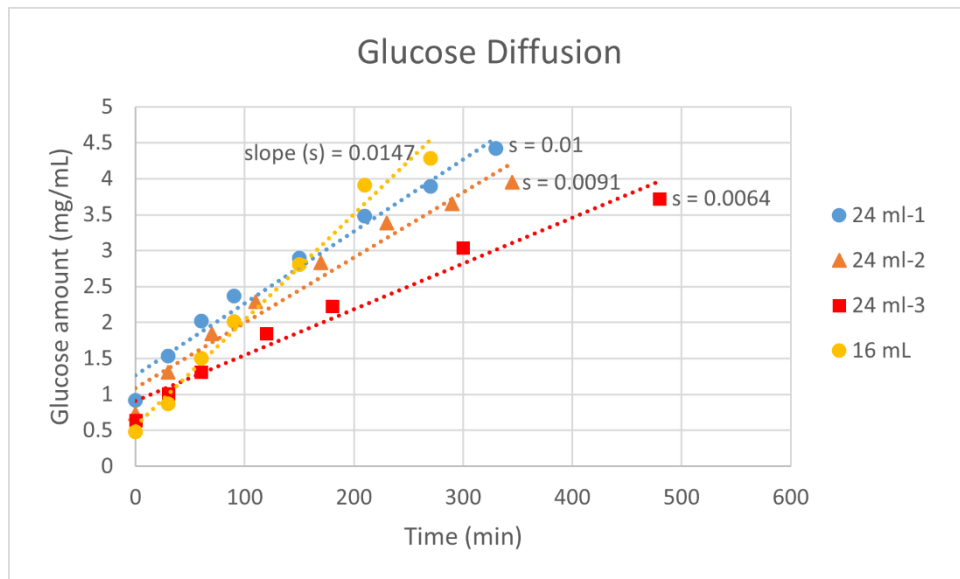
Figure 3.2.9. Glucose diffusion graph of 82 µm thick membrane repeats and, 60 µm thick membrane. The slopes of each line were measured by the line equation.

3.2.5. Mechanical Properties

To evaluate the mechanical properties of 60 and 82 µm spinnings, uniaxial tensile testing was performed. All samples of 82 µm spinning demonstrated a mechanical strength of 1.2 MPa maintaining the repeatability (Fig. 3.2.10.a). The samples of 60 µm presented a strength of 0.8 MPa on average, although the elasticity of samples had a gap of 15% strain (Fig. 3.2.10.b). When the best results of each membrane were compared, 82 µm resulted in higher strength but less elasticity than that of 60 µm (Fig. 3.2.10.c). It can also be observed from the pictures taken during the analysis in Figure 3.2.10.d that 60 µm has higher elasticity than 82 µm. These results indicate that the goal to obtain in higher strength membranes was achieved through increasing the membrane thickness.
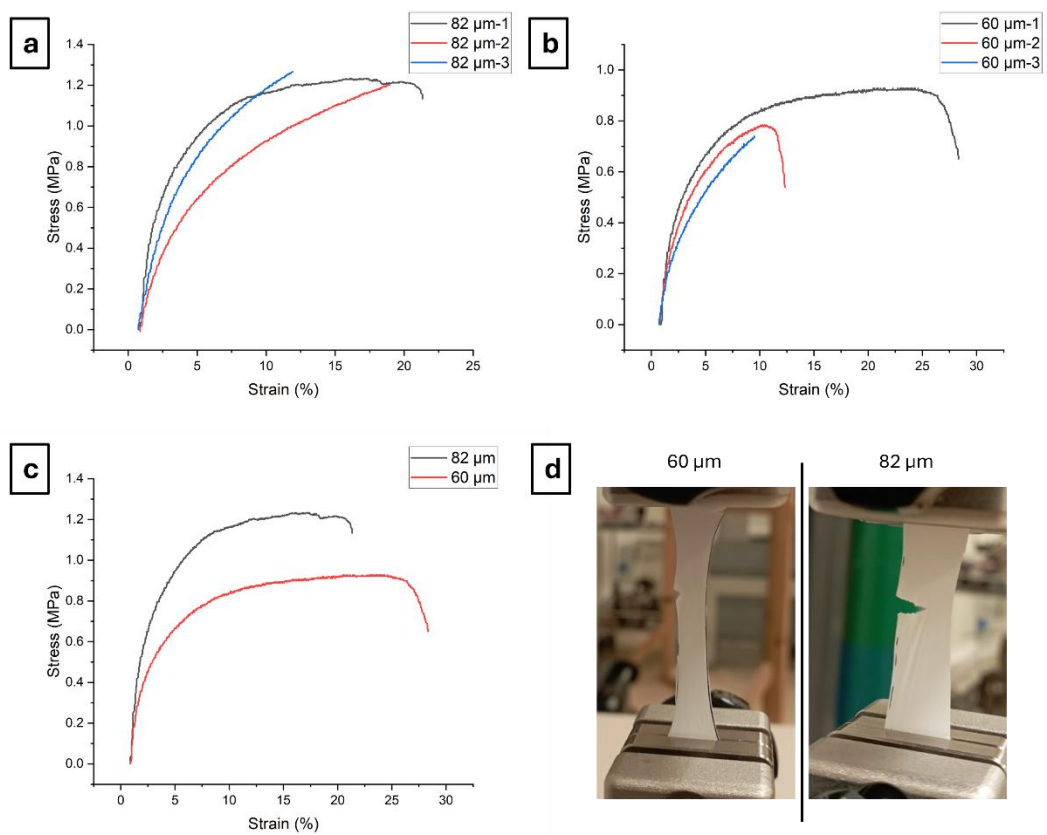
Figure 3.2.10. Mechanical strength of the membranes (a) repeats of 82 µm thick membrane, (b) repeats of 60 µm membrane, (c) comparison of 60 and 82 µm, and (d) images showing the break of membranes during tensile test

The overall stress value that membranes can withstand was calculated on average as 1000 kPa which is significantly greater than the reported highest values of 600 and 800 kPa for PGS membranes [43, 67]. The study of Mitsak et al. measured the stress values of porous PGS samples as 550 kPa with a crosslinking at 135°C for 48 h [43]. Jeffries et al. were able to increase this value to 650 kPa by increasing the temperature to 150°C for 24 h and also by obtaining a fibrous scaffold [67]. In this study, we were able to report a stress value of 1200 kPa as the highest number with a crosslinking at 160°C for 48 h proving the stability of fibrous scaffolds being higher than that of any other porous scaffolds, and higher crosslinking temperatures resulting in higher stiffness.

3.2.6. Biocompatibility Measurements

The PGS membranes were evaluated in terms of their biocompatibility with human corneal epithelial cells. Since the sterilization process of PGS membranes requires ethanol and UV radiation, the effect of ethanol incubation time was evaluated for cell attachment on the membranes. The preliminary studies resulted that HCEpCs have higher viability with the membranes sterilized with ethanol longer than 1h (not shown here). For this purpose, 2h, and overnight sterilization with ethanol were examined (Fig. 3.2.11).
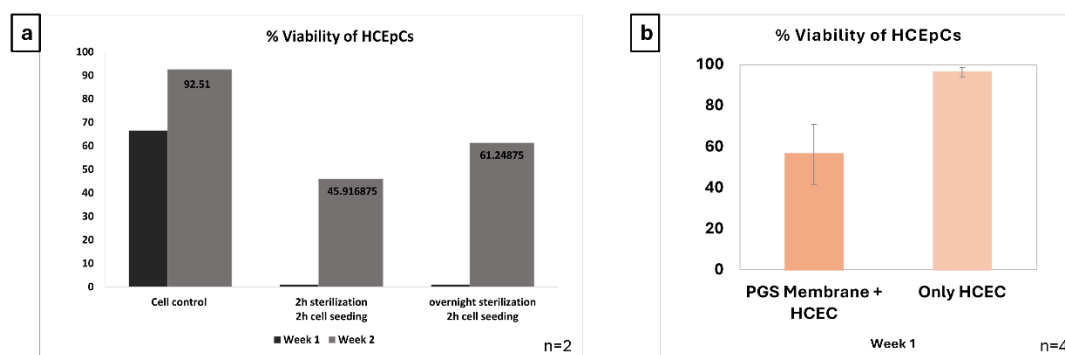
Figure 3.2.11. Biocompatibility evaluation of PGS membranes by viability assay with HCEpCs (a) sterilization time effect, **(b)** collagen coating effect

According to the viability assay data (Fig. 3.2.11.a), all groups yielded near zero viability in the first week. However, after the end of second week of culture, 2h sterilization with 2h of cell seeding incubation yielded 45% viability, and overnight sterilization with 2h of cell seeding incubation yielded 61% viability. It is clear that overnight sterilization obviously has higher effect, might be due to the wash of excess PVA from the membranes. To increase the cell attachment further, membranes were collagen coated and the same incubation methods applied. According to data in Figure 3.2.11.b, cells displayed almost 60% viability indicating that collagen coating has a positive effect on the cell attachment.

4. CONCLUSION AND FUTURE PERSPECTIVES

Various diseases related to cornea such as corneal degeneration, keratitis, fuch's dystrophy and corneal infections limit vision or causes vision loss. Therefore, several treatments including tissue engineering have been applied for corneal treatments. Here, we combined PGS with a nontoxic polymer PVA by an optimized electrospinning and obtained a fibrous and porous membrane for corneal membrane mimicking. The elevated curing temperature of 160°C increased the crosslinking density and yielded uniform fibers without collapsing into the collector sheet. Then, the PVA removal was achieved to obtain higher transparency by longer washing in water and by additional rinse in ethanol. The rise in the thickness of the membranes provided a mechanical strength in terms of toughness and elasticity which is a desirable property for corneal tissue engineering materials. The permeability of the produced membrane was promising when compared to real cornea tissue. By this approach we produced a tough membrane while avoiding many of the cytotoxicity concerns related to curing and purification processes used in earlier electrospinning processes for PGS.

The prepared PGS membranes have the problem of being less transparent than the natural cornea transparency. This problem might be solved with the cell proliferation and production of collagen and proteoglycans for Bowman and Descemet's membranes. This requires the degradation of membranes; therefore, degradation mechanics of the membrane can be further investigated. We have not achieved this with 2 weeks of cell culture. Thus, longer cell culture periods or in vivo applications would help to understand the degradation mechanism and obtain transparency. Another solution for this problem can be the acrylation or methacrylation of PGS so that viscosity of PGS can be increased and it can be electrospun by itself. By this way, additional polymers such as PVA does not interrupt the transparency and clearness of the artificial cornea membranes.

5. BIBLIOGRAPHY

1. Ghezzi, C.E., J. Rnjak-Kovacina, and D.L. Kaplan, *Corneal tissue engineering: recent advances and future perspectives.* Tissue Engineering Part B: Reviews, 2015. **21**(3): p. 278-287.
2. Almubrad, T. and S. Akhtar, *Structure of corneal layers, collagen fibrils, and proteoglycans of tree shrew cornea.* Molecular vision, 2011. **17**: p. 2283.
3. DelMonte, D.W. and T. Kim, *Anatomy and physiology of the cornea.* Journal of Cataract & Refractive Surgery, 2011. **37**(3): p. 588-598.
4. Cutler, T.J., *Corneal epithelial disease.* Veterinary Clinics: Equine Practice, 2004. **20**(2): p. 319-343.
5. Torricelli, A.A., et al., *The corneal epithelial basement membrane: structure, function, and disease.* Investigative ophthalmology & visual science, 2013. **54**(9): p. 6390-6400.
6. Bowman, W., *Lectures on the Parts Concerned in the Operations on the Eye; and on the Structure of the Retina ... To which are Added, a Paper on the Vitreous Humor; and Also a Few Cases of Ophthalmic Disease*. 1849: Longman, Brown, Green, and Longmans.
7. Winkler, M., et al., *Nonlinear optical macroscopic assessment of 3-D corneal collagen organization and axial biomechanics.* Investigative ophthalmology & visual science, 2011. **52**(12): p. 8818-8827.
8. Zhang, B., et al., *3D bioprinting for artificial cornea: Challenges and perspectives.* Medical engineering & physics, 2019. **71**: p. 68-78.
9. Maurice, D.M., *The structure and transparency of the cornea.* The Journal of physiology, 1957. **136**(2): p. 263.
10. Ruberti, J.W., A. Sinha Roy, and C.J. Roberts, *Corneal biomechanics and biomaterials.* Annual review of biomedical engineering, 2011. **13**: p. 269-295.
11. Gipson, I.K., S.J. Spurr-Michaud, and A.S. Tisdale, *Hemidesmosomes and anchoring fibril collagen appear synchronously during development and wound healing.* Developmental biology, 1988. **126**(2): p. 253-262.
12. Geroski, D.H., et al., *Pump function of the human corneal endothelium: effects of age and cornea guttata.* Ophthalmology, 1985. **92**(6): p. 759-763.
13. Bonanno, J.A., *Identity and regulation of ion transport mechanisms in the corneal endothelium.* Progress in retinal and eye research, 2003. **22**(1): p. 69-94.
14. Jeang, L.J., C.E. Margo, and E.M. Espana, *Diseases of the corneal endothelium.* Experimental eye research, 2021. **205**: p. 108495.

15. Gain, P., et al., *Global survey of corneal transplantation and eye banking.* JAMA ophthalmology, 2016. **134**(2): p. 167-173.

16. Tan, D.T. and A. Anshu, *Anterior lamellar keratoplasty:'Back to the Future'–a review.* Clinical & experimental ophthalmology, 2010. **38**(2): p. 118-127.

17. Parekh, M., et al., *Biomaterials for corneal endothelial cell culture and tissue engineering.* Journal of Tissue Engineering, 2021. **12**: p. 2041731421990536.

18. Trindade, B.L.C. and G.C. Eliazar, *Descemet membrane endothelial keratoplasty (DMEK): an update on safety, efficacy and patient selection.* Clinical Ophthalmology, 2019: p. 1549-1557.

19. Stuart, A.J., et al., *Descemet's membrane endothelial keratoplasty (DMEK) versus Descemet's stripping automated endothelial keratoplasty (DSAEK) for corneal endothelial failure.* Cochrane Database of Systematic Reviews, 2018(6).

20. Luo, H., et al., *Construction of tissue-engineered cornea composed of amniotic epithelial cells and acellular porcine cornea for treating corneal alkali burn.* Biomaterials, 2013. **34**(28): p. 6748-6759.

21. Fagerholm, P., et al., *Stable corneal regeneration four years after implantation of a cell-free recombinant human collagen scaffold.* Biomaterials, 2014. **35**(8): p. 2420-2427.

22. Lam, H. and M.R. Dana, *Corneal graft rejection.* International ophthalmology clinics, 2009. **49**(1): p. 31-41.

23. Sellami, D., et al. *Epidemiology and risk factors for corneal graft rejection.* in *Transplantation proceedings.* 2007. Elsevier.

24. Tan, D.T., et al., *Corneal transplantation.* The Lancet, 2012. **379**(9827): p. 1749-1761.

25. Ye, E.H., et al., *Advancements in Bioengineered Corneas for Vision Restoration-A Systematic Review.* Authorea Preprints, 2023.

26. Khan, M.U.A., et al., *Recent perspective of polymeric biomaterial in tissue engineering–a review.* Materials Today Chemistry, 2023. **34**: p. 101818.

27. Xu, R., et al., *Recent advances in biodegradable and biocompatible synthetic polymers used in skin wound healing.* Materials, 2023. **16**(15): p. 5459.

28. Rafat, M., et al., *PEG-stabilized carbodiimide crosslinked collagen–chitosan hydrogels for corneal tissue engineering.* Biomaterials, 2008. **29**(29): p. 3960-3972.

29. Liu, W., et al., *Recombinant human collagen for tissue engineered corneal substitutes.* Biomaterials, 2008. **29**(9): p. 1147-1158.

30. Fagerholm, P., et al., *A biosynthetic alternative to human donor tissue for inducing corneal regeneration: 24-month follow-up of a phase 1 clinical study.* Science translational medicine, 2010. **2**(46): p. 46ra61-46ra61.

31. Salehi, S., et al., *Characterization of structural, mechanical and nano-mechanical properties of electrospun PGS/PCL fibers.* Rsc Advances, 2014. **4**(33): p. 16951-16957.

32. Kruse, M., et al., *Electro-spun membranes as scaffolds for human corneal endothelial cells.* Current eye research, 2018. **43**(1): p. 1-11.

33. Tang, Z., Y. Akiyama, and T. Okano, *Recent development of temperature-responsive cell culture surface using poly (N-isopropylacrylamide).* Journal of Polymer Science Part B: Polymer Physics, 2014. **52**(14): p. 917-926.

34.   Wang, Y., et al., *A tough biodegradable elastomer.* Nature biotechnology, 2002. **20**(6): p. 602-606.

35.   Rai, R., et al., *Synthesis, properties and biomedical applications of poly (glycerol sebacate)(PGS): A review.* Progress in polymer science, 2012. **37**(8): p. 1051-1078.

36.   Pritchard, C.D., et al., *The use of surface modified poly (glycerol-co-sebacic acid) in retinal transplantation.* Biomaterials, 2010. **31**(8): p. 2153-2162.

37.   Salehi, S., et al., *Fabrication and characterization of biodegradable polymeric films as a corneal stroma substitute.* Advanced biomedical research, 2015. **4**.

38.   Kemppainen, J.M. and S.J. Hollister, *Tailoring the mechanical properties of 3D-designed poly (glycerol sebacate) scaffolds for cartilage applications.* Journal of Biomedical Materials Research Part A: An Official Journal of The Society for Biomaterials, The Japanese Society for Biomaterials, and The Australian Society for Biomaterials and the Korean Society for Biomaterials, 2010. **94**(1): p. 9-18.

39.   Razzaq, M.Y., et al., *Shape-memory polymer medical devices*, in *Encyclopedia of Biomedical Engineering, Biomaterials: Biomaterial Applications and Advanced Medical Technologies*. 2019, Elsevier. p. 394-405.

40.   Godinho, B., N. Gama, and A. Ferreira, *Different methods of synthesizing poly (glycerol sebacate)(PGS): A review.* Frontiers in Bioengineering and Biotechnology, 2022. **10**: p. 1033827.

41.   Krook, N.M., et al., *In vitro examination of poly (glycerol sebacate) degradation kinetics: Effects of porosity and cure temperature.* International Journal of Polymeric Materials and Polymeric Biomaterials, 2019.

42.   Chen, J.-S., et al., *Controlled degradation of epoxy networks: analysis of crosslink density and glass transition temperature changes in thermally reworkable thermosets.* Polymer, 2004. **45**(6): p. 1939-1950.

43.   Mitsak, A.G., A.M. Dunn, and S.J. Hollister, *Mechanical characterization and non-linear elastic modeling of poly (glycerol sebacate) for soft tissue engineering.* Journal of the mechanical behavior of biomedical materials, 2012. **11**: p. 3-15.

44.   Ding, X., et al., *Control the mechanical properties and degradation of poly (glycerol sebacate) by substitution of the hydroxyl groups with palmitates.* Macromolecular bioscience, 2020. **20**(9): p. 2000101.

45.   Pomerantseva, I., et al., *Degradation behavior of poly (glycerol sebacate).* Journal of Biomedical Materials Research Part A: An Official Journal of The Society for Biomaterials, The Japanese Society for Biomaterials, and The Australian Society for Biomaterials and the Korean Society for Biomaterials, 2009. **91**(4): p. 1038-1047.

46.   Wang, Y., Y.M. Kim, and R. Langer, *In vivo degradation characteristics of poly (glycerol sebacate).* Journal of Biomedical Materials Research Part A: An Official Journal of The Society for Biomaterials, The Japanese Society for Biomaterials, and The Australian Society for Biomaterials and the Korean Society for Biomaterials, 2003. **66**(1): p. 192-197.

47.   Liang, S.-L., et al., *In vitro enzymatic degradation of poly (glycerol sebacate)-based materials.* Biomaterials, 2011. **32**(33): p. 8486-8496.

48. Chen, Q.-Z., et al., *Characterisation of a soft elastomer poly (glycerol sebacate) designed to match the mechanical properties of myocardial tissue.* Biomaterials, 2008. **29**(1): p. 47-57.

49. Kafouris, D., et al., *Biosourced amphiphilic degradable elastomers of poly (glycerol sebacate): Synthesis and network and oligomer characterization.* Macromolecules, 2013. **46**(3): p. 622-630.

50. Liu, Q., et al., *Preparation and characterization of a thermoplastic poly (glycerol sebacate) elastomer by two-step method.* Journal of applied polymer science, 2007. **103**(3): p. 1412-1419.

51. Patel, A., et al., *Highly elastomeric poly (glycerol sebacate)-co-poly (ethylene glycol) amphiphilic block copolymers.* Biomaterials, 2013. **34**(16): p. 3970-3983.

52. Ning, Z., et al., *Lipase-catalyzed synthesis and characterization of poly (glycerol sebacate).* Biomacromolecules, 2021. **23**(1): p. 398-408.

53. Lang, K., et al., *Enzymatic polymerization of poly (glycerol-1, 8-octanediol-sebacate): Versatile poly (glycerol sebacate) analogues that form monocomponent biodegradable fiber scaffolds.* Biomacromolecules, 2020. **21**(8): p. 3197-3206.

54. Perin, G.B. and M.I. Felisberti, *Enzymatic synthesis of poly (glycerol sebacate): Kinetics, chain growth, and branching behavior.* Macromolecules, 2020. **53**(18): p. 7925-7935.

55. Chen, Q.-Z., et al., *An elastomeric patch derived from poly (glycerol sebacate) for delivery of embryonic stem cells to the heart.* Biomaterials, 2010. **31**(14): p. 3885-3893.

56. Gao, J., et al., *Poly (glycerol sebacate) supports the proliferation and phenotypic protein expression of primary baboon vascular cells.* Journal of Biomedical Materials Research Part A: An Official Journal of The Society for Biomaterials, The Japanese Society for Biomaterials, and The Australian Society for Biomaterials and the Korean Society for Biomaterials, 2007. **83**(4): p. 1070-1075.

57. Frydrych, M., et al., *Biomimetic poly (glycerol sebacate)/poly (l-lactic acid) blend scaffolds for adipose tissue engineering.* Acta Biomaterialia, 2015. **18**: p. 40-49.

58. Pritchard, C.D., et al., *Retinal transplantation using surface modified poly (glycerol-co-sebacic acid) membranes.* Biomaterials, 2010. **31**(31): p. 7978-7984.

59. Salehi, S., et al., *Poly (glycerol sebacate)-poly (ε-caprolactone) blend nanofibrous scaffold as intrinsic bio-and immunocompatible system for corneal repair.* Acta biomaterialia, 2017. **50**: p. 370-380.

60. Salehi, S., et al., *New nanofibrous scaffold for corneal tissue engineering.* Klinische Monatsblatter fur Augenheilkunde, 2014. **231**(6): p. 626-630.

61. Stafiej, P., et al., *Comparative results of cell culture of human corneal epithelial cells (HCE) and human corneal keratocytes (HCK) on electrospun nanofiber matrices of Polycaprolactone blended with Poly (glycerol sebacate) and chitosan.* Investigative Ophthalmology & Visual Science, 2016. **57**(12): p. 1263-1263.

62. Van Vlierberghe, S., P. Dubruel, and E. Schacht, *Biopolymer-based hydrogels as scaffolds for tissue engineering applications: a review.* Biomacromolecules, 2011. **12**(5): p. 1387-1408.

63.   Fatimi, A., et al., *Natural hydrogel-based bio-inks for 3D bioprinting in tissue engineering: A review.* Gels, 2022. **8**(3): p. 179.

64.   Yeh, Y.-C., et al., *3D printing of photocurable poly (glycerol sebacate) elastomers.* Biofabrication, 2016. **8**(4): p. 045004.

65.   Wu, Y.-L., et al., *Three-dimensional printing of poly (glycerol sebacate) acrylate scaffolds via digital light processing.* ACS Applied Bio Materials, 2020. **3**(11): p. 7575-7588.

66.   Zhu, S., et al., *Recent advances in patterning natural polymers: from nanofabrication techniques to applications.* Small Methods, 2021. **5**(3): p. 2001060.

67.   Jeffries, E.M., et al., *Highly elastic and suturable electrospun poly (glycerol sebacate) fibrous scaffolds.* Acta biomaterialia, 2015. **18**: p. 30-39.

68.   Gultekinoglu, M., et al., *Preparation of poly (glycerol sebacate) fibers for tissue engineering applications.* European Polymer Journal, 2019. **121**: p. 109297.

69.   Wilk, S. and A. Benko, *Advances in fabricating the electrospun biopolymer-based biomaterials.* Journal of Functional Biomaterials, 2021. **12**(2): p. 26.

70.   Ashammakhi, N., et al., *Advancing tissue engineering by using electrospun nanofibers.* 2008.

71.   Finne-Wistrand, A., et al., *Resorbable Scaffolds from Three Different Techniques: Electrospun Fabrics, Salt-Leaching Porous Films, and Smooth Flat Surfaces.* Macromolecular bioscience, 2008. **8**(10): p. 951-959.

72.   Deitzel, J.M., et al., *The effect of processing variables on the morphology of electrospun nanofibers and textiles.* Polymer, 2001. **42**(1): p. 261-272.

73.   Ding, B., et al., *Preparation and characterization of a nanoscale poly (vinyl alcohol) fiber aggregate produced by an electrospinning method.* Journal of Polymer Science Part B: Polymer Physics, 2002. **40**(13): p. 1261-1268.

74.   Zhang, C., et al., *Study on morphology of electrospun poly (vinyl alcohol) mats.* European polymer journal, 2005. **41**(3): p. 423-432.

75.   Haghi, A. and M. Akbari, *Trends in electrospinning of natural nanofibers.* physica status solidi (a), 2007. **204**(6): p. 1830-1834.

76.   Hanuman, S., et al., *Electrospinning for biomedical applications*, in *Advances in Biomedical Polymers and Composites*. 2023, Elsevier. p. 433-464.

77.   Bhardwaj, N. and S.C. Kundu, *Electrospinning: A fascinating fiber fabrication technique.* Biotechnology advances, 2010. **28**(3): p. 325-347.

78.   Yi, F. and D.A. LaVan, *Poly (glycerol sebacate) nanofiber scaffolds by core/shell electrospinning.* Macromolecular bioscience, 2008. **8**(9): p. 803-806.

79.   Hu, J., et al., *Electrospinning of poly (glycerol sebacate)-based nanofibers for nerve tissue engineering.* Materials Science and Engineering: C, 2017. **70**: p. 1089-1094.

80.   Gaharwar, A.K., et al., *Anisotropic poly (glycerol sebacate)-poly (ϵ-caprolactone) electrospun fibers promote endothelial cell guidance.* Biofabrication, 2014. **7**(1): p. 015001.

81.   Denis, P., et al., *Poly (Glycerol sebacate)–poly (l-lactide) nonwovens. Towards attractive electrospun material for tissue engineering.* Polymers, 2019. **11**(12): p. 2113.

82.   Chaouat, M., et al., *A novel cross-linked poly (vinyl alcohol)(PVA) for vascular grafts.* Advanced Functional Materials, 2008. **18**(19): p. 2855-2861.

83.   Saudi, A., et al., *Promoting neural cell proliferation and differentiation by incorporating lignin into electrospun poly (vinyl alcohol) and poly (glycerol sebacate) fibers.* Materials Science and Engineering: C, 2019. **104**: p. 110005.

84.   Saudi, A., et al., *Design and fabrication of poly (glycerol sebacate)-based fibers for neural tissue engineering: Synthesis, electrospinning, and characterization.* Polymers for Advanced Technologies, 2019. **30**(6): p. 1427-1440.

85.   Myung, D., et al., *Glucose permeability of human, bovine, and porcine corneas in vitro.* Ophthalmic Research, 2006. **38**(3): p. 158-163.

86.   Jaafar, I.H., et al., *Spectroscopic evaluation, thermal, and thermomechanical characterization of poly (glycerol-sebacate) with variations in curing temperatures and durations.* Journal of materials science, 2010. **45**: p. 2525-2529.

87.   Liu, J. and C.J. Roberts, *Influence of corneal biomechanical properties on intraocular pressure measurement: quantitative analysis.* Journal of Cataract & Refractive Surgery, 2005. **31**(1): p. 146-155.

88.   Ehlers, N., T. Bramsen, and S. Sperling, *Applanation tonometry and central corneal thickness.* Acta ophthalmologica, 1975. **53**(1): p. 34-43.

89.   Salehi, S., et al., *Generation of PGS/PCL blend nanofibrous scaffolds mimicking corneal stroma structure.* Macromolecular Materials and Engineering, 2014. **299**(4): p. 455-469.

APPENDIX A

Table A. The GPC results of prePGS indicating the number of chains in the identified MW as **peak area**, the ratio of that area to summation of all areas as **% peak area, MW, MN** and **PDI**

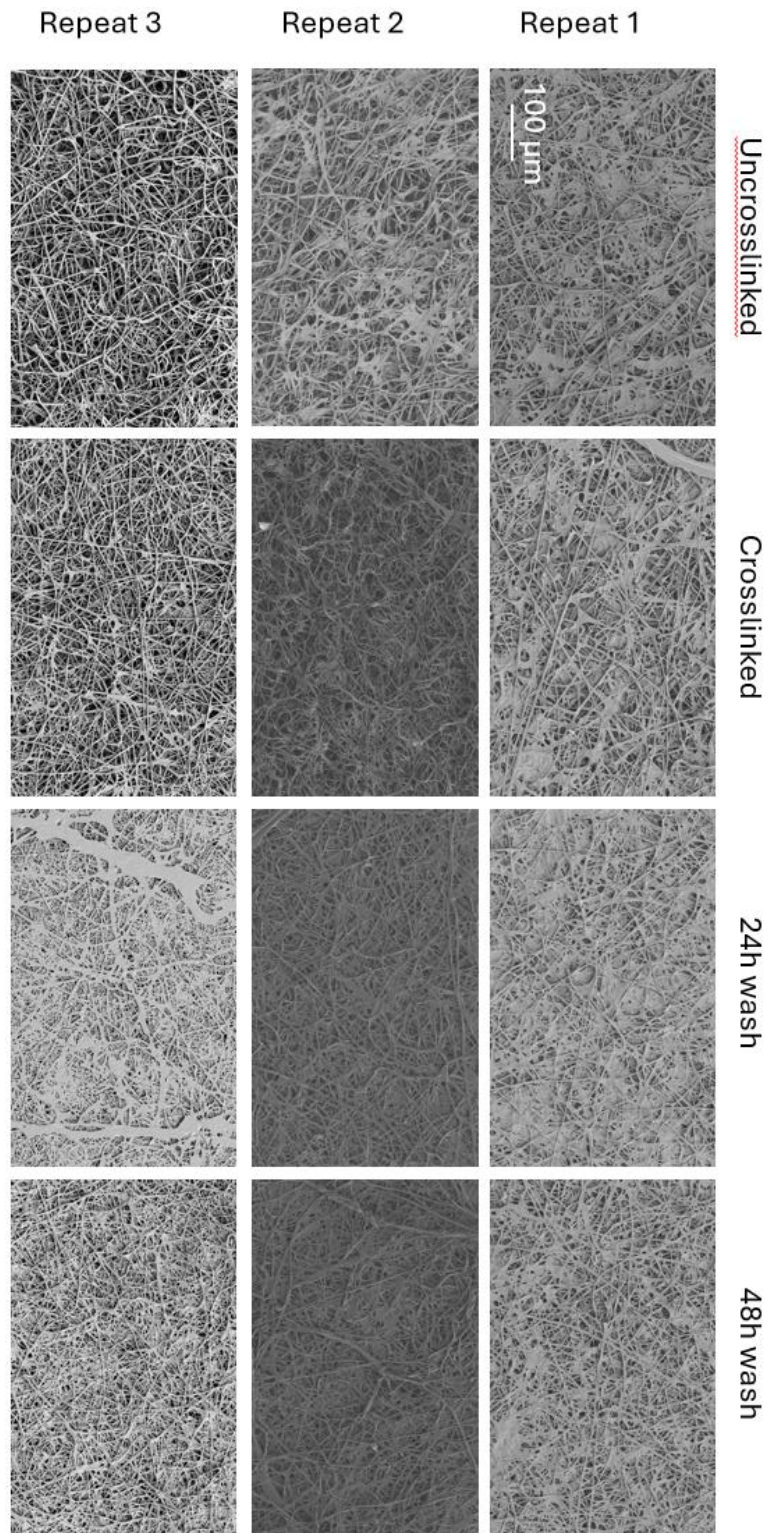| Peak Area (mV.s)	% Peak Area	Mw (g/mol)	Mn (g/mol)	Mw/Mn (PDI)
271.9527	29.76262	53127	46484	1.142909
460.0321	50.34612	9380	6076	1.543779
45.02763	4.927843	2049	2039	1.004904
49.53579	5.421219	1529	1517	1.00791
50.7222	5.551059	1037	1024	1.012695
36.46856	3.991135	625	616	1.01461

Figure B. 24 mL spin repeats comparison with uncrosslinked, crosslinked, 24h washed and 48h washed membrane SEM images